A noncanonical GTPase signaling mechanism controls exit from mitosis in budding yeast.

Xiaoxue Zhou[1,*], Shannon Y. Weng, Stephen P. Bell, Angelika Amon

[1]Department of Biology, David H. Koch Institute for Integrative Cancer Research, Howard Hughes Medical Institute, Massachusetts Institute of Technology, Cambridge, MA 02139, USA

[*]Correspondence to: snow.zhou@nyu.edu
Present address: Department of Biology, New York University, New York, NY

ABSTRACT

In the budding yeast *Saccharomyces cerevisiae*, exit from mitosis is coupled to spindle position to ensure successful genome partitioning between mother and daughter cell. This coupling occurs through a GTPase signaling cascade known as the mitotic exit network (MEN). The MEN senses spindle position via a Ras-like GTPase Tem1 which primarily localizes to the spindle pole bodies (SPBs, yeast equivalent of centrosomes) during anaphase. How Tem1 couples the status of spindle position to MEN activation is not fully understood. Here, we show that Tem1 does not function as a molecular switch as its nucleotide state does not change upon MEN activation. Instead, Tem1's nucleotide state regulates its SPB localization to establish a concentration difference in the cell in response to spindle position. By artificially tethering Tem1 to the SPB, we demonstrate that the essential function of $Tem1^{GTP}$ is to localize Tem1 to the SPB. Tem1 localization to the SPB primarily functions to generate a high effective concentration of Tem1 and MEN signaling can be initiated by concentrating Tem1 in the cytoplasm with genetically encoded multimeric nanoparticles. This localization/concentration-based GTPase signaling mechanism for Tem1 differs from the canonical Ras-like GTPase signaling paradigm and is likely relevant to other localization-based signaling scenarios.

INTRODUCTION

Small GTPases are key regulators in many cellular processes including cell signaling, actin organization, and membrane trafficking[1]. They typically function as molecular switches whose interaction with downstream effectors are regulated by changing nucleotide state[2]. Their high affinity for guanine nucleotides and low intrinsic GTP hydrolysis and GDP/GTP exchange activities underlie their success as molecular switches. Regulatory proteins such as GTPase activating proteins (GAPs) and guanine nucleotide exchange factors (GEFs) control these switches by modulating their GTP/GDP state in response to specific inputs[3]. A classic example is the founding member of the family, Ras, which regulates cell proliferation in response to growth factors[4]. Binding of growth factors to receptors at the cell surface leads to the recruitment of a GEF to the membrane, which promotes the conversion of membrane anchored Ras^{GDP} to Ras^{GTP}. Ras^{GTP} then recruits and activates downstream effectors to signal proliferation. Although well established, it is unclear whether the same switch mechanism applies to all small GTPases involved in cell signaling.

The mitotic exit network (MEN) is a GTPase signaling cascade in the budding yeast *Saccharomyces cerevisiae* that regulates the exit from mitosis where the mitotic spindle disassembles, the nucleus divides, and chromosomes decondense. In budding cells, the site of cytokinesis or division plane is specified by the bud neck prior to mitosis[5]. To ensure proper genome partitioning, the mitotic spindle must be aligned along the mother-bud axis. The spindle position checkpoint (SPoC) blocks exit from mitosis until a spindle pole successfully enters the bud (Fig. 1A). This checkpoint is executed by establishing two zones in the cell with spatially distributed proteins (an inhibitory zone in the mother compartment and an activating zone in the bud)[6,7] and a sensor, the MEN, which integrates multiple signals including spindle position to regulate cell cycle progression[8] (Fig. 1A-B). Only when a spindle pole escapes the inhibitory zone in the mother and enters the activating zone in the bud in anaphase is the MEN activated, triggering mitotic exit. If the spindle is mis-positioned and remains in the mother cell/inhibitory zone, the MEN is kept inactive, arresting the cell in anaphase. Spindle position is transmitted to the MEN through the small GTPase Tem1[9,10]. How Tem1 senses and couples spindle position to MEN activation is not well understood.

Like Ras, Tem1 undergoes a GTP/GDP nucleotide cycle and Tem1's nucleotide states play an important role in its function. Mutations that block GTP hydrolysis and lock Tem1 in the

GTP state are constitutively active and bypass the SPoC[11]. Conversely, nucleotide binding mutants that bias Tem1 toward the GDP state render the protein inactive and arrest cells in anaphase even with a correctly positioned spindle[12]. Given these findings, it has been assumed that Tem1 functions as a molecular switch like Ras and spindle position regulates Tem1 by changing its nucleotide state (Fig. 1C). However, there are several aspects of Tem1 biology that are unusual for a small GTPase.

First, while the GTP hydrolysis rate of Tem1 is accelerated by a bipartite GAP complex Bub2-Bfa1[10,13], Tem1 does not appear to require a GEF to function, likely due to a relatively fast intrinsic nucleotide exchange rate[13]. As a result, the only way to regulate Tem1's nucleotide state is by modulating the activity of the GAP. Consistent with this view, a prevailing model proposed that the MEN is activated by inactivating the GAP. The polo-like kinase Cdc5 phosphorylates Bfa1 which was shown to reduce GAP activity in vitro[14]. However, the hypothesis that regulating GAP activity controls mitotic exit has not been rigorously tested due to the lack of tools to directly assess GAP activity or Tem1's nucleotide state in the cell.

A second peculiar aspect of Tem1 is that its cellular localization is regulated and correlates with MEN activation[10,15,16] (Fig. 1A). When the spindle is correctly positioned in anaphase (MEN ON), Tem1 primarily localizes to the spindle pole body (SPB, functional equivalent of centrosomes in yeast) that moves into the bud (daughter SPB or dSPB). However, if the spindle is mis-positioned (MEN OFF), Tem1 is largely cytoplasmic. Intriguingly, Tem1 localization to the SPB is highly dynamic with a residence time of around 5 s as revealed by fluorescence recovery after photobleaching (FRAP) analysis[15,17,18]. Furthermore, forcing Tem1 localization to the SPB by artificially tethering Tem1 to a SPB component Cnm67 overrides the checkpoint (SPoC defective)[18], indicating a functional link between Tem1 localization and activity. How Tem1 localization is related to its activity, and more importantly, its nucleotide state remains unclear.

Here, we demonstrate that Tem1's nucleotide state regulates its localization, and that SPB localization controls Tem1 activity. Our results suggest that Tem1 does not function as a molecular switch like Ras, as its nucleotide state does not change upon MEN activation. Instead, the nucleotide state of Tem1 is used to establish a concentration difference between the SPB and cytosol. Only when the SPB enters the bud can Tem1 achieve the high effective concentration required to recruit and activate its downstream effector protein Cdc15. This noncanonical

GTPase signaling mechanism differs from the molecular switch paradigm described by Ras and enables Tem1 to couple a spatial cue (i.e., spindle position) to downstream signaling. The observation that localizing Tem1 to SPB/centrosomes can modulate protein-protein interactions by increasing local concentration is likely relevant to other localization-based signaling scenarios.

RESULTS

Tem1 is a noncanonical small GTPase with relatively low affinity for nucleotides.

To understand the role of Tem1's nucleotide cycle, we first characterized the biochemical properties of purified Tem1 (Fig. S1): its intrinsic GTP hydrolysis and nucleotide exchange rates, and nucleotide binding activities. Tem1 hydrolyzed GTP with $k_{hyd} = 0.011 \pm 0.001$ min^{-1} (or 1.8×10^{-4} s^{-1}, Fig. 1D) and exhibited a nucleotide exchange rate $k_{ex} = 0.005 \pm 0.0006$ s^{-1} (Fig. 1E). The hydrolysis rate is slower than those previously measured with an indirect method[11,13], whereas the exchange rate is similar and much faster than that of Ras (Fig. 1E). The fast intrinsic nucleotide exchange rate of Tem1 prompted us to examine whether Tem1 has a reduced affinity for nucleotides. Indeed, we found that Tem1 has a low micromolar affinity for MANT-GDP ($K_D = 1.2 \pm 0.1$ μM, Fig. 1F), in contrast to the picomolar to nanomolar nucleotide affinities for typical small GTPases. These results suggest that while the intrinsic GTP hydrolysis rate is low for Tem1, the fast GEF-independent nucleotide exchange renders Tem1 a self-activating molecular switch as the OFF state (Tem1^{GDP}) is unstable due to the high GTP to GDP ratio in the cell. Consequently, Tem1's nucleotide state can only be controlled by regulating GAP activity.

Tem1's nucleotide state regulates its localization.

Despite it being an unusual GTPase, Tem1's nucleotide state still regulates its activity. However, how Tem1's nucleotide state regulates its activity remains elusive. Given the correlation between Tem1's SPB localization and its activity, we first investigated whether Tem1's nucleotide state regulates its localization. To track Tem1 localization in the cell, we developed a N-terminal fluorescent Tem1 fusion (yEGFP-Tem1) that, unlike previous C-terminal fusions[16,19], shows similar expression and activity as wild-type untagged Tem1 (Fig. S2). To examine the effect of nucleotide state, we generated three mutations in Tem1 at the endogenous locus: the hydrolysis mutant Tem1Q79L (corresponding to RasQ61L) that locks Tem1 in GTP state, the nucleotide-

binding mutants Tem1T34A/N (corresponding to Ras-S17A/N in the P loop region, Fig. S2A) that bias towards the GDP or apo state, and the effector mutant Tem1T52A (corresponding to Ras-T35A at switch I region, Fig. S2A) that cannot undergo the confirmation change upon GTP binding necessary for effector recognition and thus essentially appears as "GDP-locked" for effectors. Wild-type Tem1 localizes primarily to the dSPB in metaphase and this localization is enhanced upon anaphase onset (which typically coincides with migration of the dSPB into the bud) followed by a decline as cells exit from mitosis (Fig. 2A). As previously reported[11], the GTP-locked Tem1Q79L showed stronger localization to both SPBs throughout metaphase and anaphase (Fig. 2A-C). In contrast, the inactive GDP-locked/apo mutants T34A and T34N abolished SPB localization and the effector mutant T52A significantly reduced SPB localization. These results strongly suggest that Tem1's nucleotide state specifies its SPB localization.

Tethering Tem1 to the SPB bypasses the requirement for Tem1^{GTP}.

Because nucleotide state controls Tem1 localization and localization is integral to Tem1 activity[10,15,16], we hypothesized that nucleotide-state mutations are lethal due to mis-localization. To test this idea, we asked if artificially localizing Tem1 to the SPB can restore successful cell division in Tem1 mutants defective in binding GTP. We tethered yEGFP-Tem1 to the SPB using a GFP nanobody (GFP binding protein, GBP) fused to a SPB outer plaque component Cnm67. This tethering completely rescued the lethality of both *tem1T34A/N* and *tem1T52A* (Fig. 2D). Direct fusion to Cnm67 also rescued an expanded panel of Tem1 mutants (Fig. S3B). Furthermore, when Tem1 was tethered to the SPB, cells exited from mitosis with similar kinetics regardless of the nucleotide state (Fig. 2E). These results suggests that the essential function of Tem1^{GTP} is to localize Tem1 to the SPB and that signaling downstream of Tem1 to the effector kinase Cdc15 does not require Tem1^{GTP} as long as Tem1 is correctly localized.

Localization of Tem1 to the SPB depends on the GAP Bub2-Bfa1 and effector Cdc15.

Having established that nucleotide state controls Tem1 activity by regulating its SPB localization, we next investigated how Tem1, specifically Tem1^{GTP}, is recruited to the SPB. Previous studies showed that SPB localization of Tem1 mainly depends on the bipartite GAP complex Bub2-Bfa1[10]. However, a small pool of Tem1 can localize to the SPB in a GAP-independent manner through an unknown mechanism. Using our yEGFP-Tem1 fusion and

quantitative time-lapse microscopy, we compared the localization patterns of Tem1, the GAP component Bfa1, and Tem1's effector protein Cdc15 in the presence or absence of the catalytic subunit of the GAP complex Bub2 (Fig. 3A).

Bub2 and Bfa1 form a stable complex that localizes to the SPB[10]. The GAP complex preferentially accumulates at the SPB closest to the bud (typically the dSPB) in metaphase. Upon anaphase onset, this asymmetry is exacerbated due to both an increase in localization at the dSPB and active removal of the GAP from the mSPB[17]. The latter outcome is achieved, at least in part, through phosphorylation of Bfa1 by the inhibitory zone protein Kin4[17,20], a kinase that is restricted to the mother cortex and localizes to the mSPB in anaphase[21,22]. Tem1 localization to the SPB was similar to the GAP until late anaphase, when Tem1 also localized to the mSPB (Fig. 3A). The effector Cdc15 did not localize to the SPBs until anaphase onset and showed only a moderate bias toward dSPB. Bfa1 does not localize to either SPBs in the absence of Bub2[10] (Fig. 3A). In contrast, Tem1 and Cdc15 showed synchronized and symmetric localization to both SPBs in late anaphase in *bub2Δ* cells (Fig. 3A, Fig. S4D). Similar localization patterns for Tem1 were found in *bfa1Δ* or *bfa1Δbub2Δ* double mutants (Fig. S4A-C). Furthermore, the GTP-locked mutant Tem1Q79L showed a similar localization profile and anaphase progression as wild-type Tem1 in the absence of the GAP (Fig. S4A-B), consistent with our prediction that as a self-activating GTPase, Tem1 is mainly in the GTP bound state without the GAP.

Given the correlated localization between Tem1 and Cdc15 in *bub2Δ* cells, we hypothesized that in the absence of the GAP, Tem1 (mainly $Tem1^{GTP}$) and Cdc15 form a complex that is recruited to the SPB. In this model, Tem1 and Cdc15 localization to the SPB should be interdependent (Fig. 3B). It is well established that Cdc15 localization depends on Tem1[16], leading us to examine the role of Cdc15 in Tem1 localization: we either depleted Cdc15 with the auxin-inducible degron system[23] (Fig. 3C-D) or generated *cdc15Δ* strains kept alive with a hyperactive *DBF2* allele[24] (Fig. S5A-B). In the degron strain, Cdc15 depletion was nearly complete and arrested cells in anaphase (Fig. 3C). Tem1 localization to dSPB was not affected by Cdc15 depletion or deletion in *BFA1* cells, but was completely dependent on Cdc15 in *bfa1Δ* cells. Similar results were observed for Tem1Q79L (Fig. S5C), demonstrating that Tem1 ($Tem1^{GTP}$) cannot localize to the SPB on its own and relies on either the GAP or Cdc15 for recruitment to the SPB.

The GAP complex Bub2-Bfa1 preferentially binds Tem1^{GTP}.

Given that SPB localization of Tem1 depends on its GAP (Bub2-Bfa1) and its effector (Cdc15) and Tem1's nucleotide state regulates its SPB localization, we hypothesized that the GAP and Cdc15 recruit specifically Tem1^{GTP}. To test whether interaction between Tem1 and the GAP is nucleotide dependent, we first performed co-immunoreaction between different Tem1 nucleotide mutants and the GAP using yEGFP-Tem1 and Bfa1-3V5 fusions. As shown previously[11], GTP-locked Tem1Q79L interacted more strongly with the GAP than wild-type Tem1 (Fig. 4A). More importantly, the GDP-locked/apo mutant Tem1T34A/N and the effector mutant Tem1T52A had significantly reduced affinity for the GAP: almost no Bfa1-3V5 was pulled down by yEGFP-Tem1 with these mutations (Fig. 4A). These results strongly support our hypothesis that the GAP complex recruits specifically Tem1^{GTP} to the SPB.

To better characterize the interaction between the GAP and Tem1, we developed an interaction assay using AlphaLISA[25], a bead-based technology that reports on biomolecular interactions. We mixed recombinant biotinylated Tem1 loaded with either GTPγS or GDP with Bub2/Bfa1-eGFP from yeast lysate. Their interaction was detected with a pair of beads that bind each component respectively and produce proximity-based luminescence upon interaction (Fig. 4C). Titrating biotinylated Tem1 in this assay revealed a strong preference of the GAP complex for Tem1^{GTP} with several orders of magnitude difference in affinity (Fig. 4D, see 10% bound line): binding between the GAP to Tem1$^{GTP\gamma S}$ was readily detected even with < 0.1 nM biotinylated Tem1, while binding between the GAP and Tem1^{GDP} was barely detectable even with 100 nM Tem1. We further dissected the contribution of each GAP subunit to the Tem1 interaction (Fig. 4G-H). While Bub2 did not interact with Tem1 in the absence of Bfa1, Bfa1 bound similarly to Tem1$^{GTP\gamma S}$ in the presence or absence of Bub2. Interestingly, Bfa1 showed increased affinity for Tem1^{GDP} in the absence of Bub2, suggesting that Bfa1 alone and Bub2-Bfa1 complex interact with Tem1 differently. We concluded that the GAP complex specifically interacts with Tem1^{GTP} and as a result leads to nucleotide dependent localization of Tem1 to the dSPB.

The effector protein Cdc15 has a relatively weak preference for Tem1^{GTP}.

We next examined the interaction between Tem1 and its effector Cdc15. As an effector, we expected Cdc15 to have a strong preference for Tem1^{GTP}. On the other hand, our SPB tethering

experiment (Fig. 2D-E) suggested that Cdc15 might not have a strict preference for Tem1^{GTP}. Indeed, in co-immunoprecipitation assays Cdc15 had a reduced affinity for the GTP-locked Tem1Q79L compared to wild-type Tem1 and retained considerable affinity for the GDP-locked/apo Tem1T34A/N and effector mutant Tem1T52A (Fig. 4B, Fig. S6A). Compared to the GAP, Cdc15 also had both lower affinity for Tem1$^{GTP\gamma S}$ and higher affinity for Tem1^{GDP} in the AlphaLISA assay (Fig. 4D and E, compare Tem1 concentration yielding 10% bound).

We estimated the binding affinity of the GAP complex to Tem1$^{GTP\gamma S}$ ($K_D < 0.4 \pm 0.2$ nM) and Cdc15 to Tem1$^{GTP\gamma S}$ ($K_D = 3.9 \pm 0.8$ nM) and Tem1^{GDP} ($K_D = 16 \pm 3$ nM) using a competition binding assay with unlabeled Tem1 (Fig. 4F). We note that the difference between Tem1$^{GTP\gamma S}$ and Tem1^{GDP} Cdc15 interaction was larger in direct binding assays (Fig. 4E) than in the competition assay (Fig. 4F). It is possible that the competition assay could be dominated by a subpopulation of Cdc15 with higher affinity. The observed weak nucleotide preference of Cdc15 is further supported by the AlphaFold predicted Cdc15-Tem1 interaction[26] (Fig. S6B) where the binding interface is away from the nucleotide binding pocket of Tem1. Based on their distinct nucleotide preference and sensitivity to mutations in Tem1, our results further suggest that Cdc15 and the GAP complex do not share the same binding interface on Tem1. We concluded that Cdc15 is a noncanonical GTPase effector protein with only a weak preference for Tem1^{GTP} over Tem1^{GDP}.

GAP stimulated GTP hydrolysis drives the fast turnover of Tem1 at the dSPB.

Now that we have established the GAP specifically recruits Tem1^{GTP} to the dSPB, we reasoned that the rapid turnover of Tem1 at the SPB observed previously could be a result of GAP-stimulated GTP hydrolysis and consequent dissociation of Tem1^{GDP}. We performed FRAP analysis to compare turnover of wild-type Tem1 and the hydrolysis deficient Tem1Q79L mutant at the dSPB (Fig. 5A) in cells arrested in anaphase by depleting Cdc15. We depleted Cdc15 to avoid potential interference of Cdc15 mediated SPB localization of Tem1, although we did not observe significant difference for Tem1 dynamics at the dSPB in anaphase cells with or without Cdc15 depletion (Fig. S7A). Inhibiting GTP hydrolysis with Tem1Q79L increased the residence time of Tem1 at the dSPB from $t_{1/2} = 6$ ($\pm$ 2) s to $t_{1/2} = 16$ ($\pm$ 7) s (Fig. 4B). A similar increase in residence time was observed in cells with a catalytically dead GAP mutant *bub2R85A* (Fig. S7B). Thus, GAP-stimulated GTP hydrolysis drives the rapid turnover of Tem1 at the dSPB.

Moreover, this finding allows us to use Tem1 residence time at the dSPB to estimate *in vivo* GAP activity as the difference of turnover rate between Tem1 and Tem1Q79L.

The GAP is not inactivated in anaphase.

It has been proposed that regulation of GAP activity, presumably by Cdc5 phosphorylation of Bfa1 at the SPB[14], could regulate Tem1 in response to spindle position. Testing this hypothesis requires a way to assess Bub2-Bfa1's GAP activity *in vivo*. We can now use Tem1 FRAP analysis to estimate the GAP-stimulated hydrolysis rate k_{hyd} as the difference of turnover rate between Tem1 and Tem1Q79L ($k_{hyd} = \ln 2/t_{1/2}^{\mathrm{Tem1}} - \ln 2/t_{1/2}^{\mathrm{Tem1Q79L}}$, Fig. 5A) which was 0.07 s^{-1}. This is about 400-fold faster than Tem1's intrinsic GTP hydrolysis rate, indicating that the GAP is active in anaphase.

If correct anaphase delivery of the dSPB to the bud downregulates the GAP to promote Tem1 and MEN activation, then Tem1 residence time at the SPB should lengthen in anaphase. This however was not the case. Similar to previous reports[15,17,18], we did not observe a significant difference in Tem1's turnover rate at the SPB between metaphase and anaphase (Fig. 5C). As the turnover of Tem1 at dSPB is mainly driven by GAP-stimulated GTP hydrolysis, this result indicates that Bub2-Bfa1's GAP activity at the SPB is not downregulated in anaphase compared to metaphase as previously assumed.

Tem1's nucleotide state does not change upon MEN activation.

If the GAP is not inactivated in anaphase, does Tem1's nucleotide state (ratio of $\mathrm{Tem1}^{\mathrm{GTP}}$ to $\mathrm{Tem1}^{\mathrm{GDP}}$ in the cell) change between metaphase and anaphase? Assuming that Tem1 undergoes spontaneous GEF-independent nucleotide exchange and GAP-stimulated GTPase hydrolysis, the parameters we measured experimentally combined with cellular concentrations of Tem1 and Bub2-Bfa1 from the literature[27] (Fig. S8) allowed us to calculate that < 10% of Tem1 is in the GTP-bound state in the presence of active GAP, while 97% of Tem1 is in the GTP bound state in the absence of the GAP (Fig. S8A). These ratios are predicted to stay the same between metaphase and anaphase given that GAP activity is not downregulated in anaphase.

To validate our conclusions, we sought to assess Tem1's nucleotide state directly. Given that the GAP Bub2-Bfa1 specifically recruits $\mathrm{Tem1}^{\mathrm{GTP}}$ to the dSPB, we reasoned that enrichment of Tem1 at the dSPB, mainly set by the fraction of SPB localized GAP bound to Tem1, should

correlate with cellular Tem1^{GTP} concentration ([Tem1^{GTP}]) and thus can serve as an indicator for [Tem1^{GTP}]. Consistent with this hypothesis, the GTP-locked Tem1Q79L has dramatically enhanced SPB localization (Fig. 2B) due to high [Tem1^{GTP}]. Interestingly, for wild-type Tem1, we observed a noticeable increase in dSPB enrichment upon anaphase onset that could be attributed to either an increase in [Tem1^{GTP}] due to an unknown GEF activity or a change in the number of Tem1 receptors at the dSPB (the GAP Bub2-Bfa1). We favor the latter interpretation as the GAP complex is redistributed from the mSPB to the dSPB upon anaphase onset (Fig. 3A). To examine the role of GAP redistribution, we immobilized the GAP by tethering the complex to the SPB using a *SPC72-BFA1* fusion[11]. This fusion retained GAP activity (Fig. S9) and abolished the increase in Tem1's localization at dSPB upon anaphase onset (Fig. 5D), confirming that the increase we observed in wild-type cells is due to an increase in the amount of GAP at the dSPB, not changes in [Tem1^{GTP}]. We further validated this finding by comparing dSPB localization of Tem1, Tem1Q79L (maximum binding), and Bfa1 (receptor) in cells with Cdc15 depleted (Fig. 5E). All three proteins increased dSPB localization upon anaphase onset synchronously due to redistribution of the GAP, and most importantly, the relative ratio between Tem1 and Tem1Q79L or Bfa1, which represents the fraction of GAP at dSPB bound to Tem1^{GTP}, remained unchanged (Fig. 5F).

These results strongly suggest that the nucleotide state of Tem1 (ratio of [Tem1^{GTP}] to [Tem1^{GDP}]) is not modulated to control MEN activation in anaphase and the majority of Tem1 in the cell remains in the GDP bound state in both metaphase (MEN inactive) and anaphase (MEN active). We showed earlier that Tem1's nucleotide state controls its activity through regulating localization. Given that Tem1's nucleotide state does not change, how does its localization change in response to spindle position? We think that it is mainly by changing the localization of its SPB receptor, the GAP, which is actively removed from the SPB that remains in the mother compartment. Only when a SPB escapes the inhibitory zone in anaphase, which indicates the correct spindle position, would the GAP and thus Tem1 accumulate at the SPB thus coupling Tem1 localization to spindle position.

MEN activity is sensitive to Tem1 concentration.

How does SPB localization of Tem1 result in Cdc15 activation? Cdc15's kinase activity is not cell cycle regulated[28]. Instead, Cdc15 is thought to be mainly regulated by SPB localization

because its scaffold protein Nud1[29] is a core component of the SPB. Thus, it was proposed that Tem1 activates Cdc15 by recruiting it to the SPB. Indeed, localization of Cdc15 to the SPB typically depends on Tem1[16]. However, this model could not explain the GAP-independent mode of SPB localization for Tem1 and Cdc15 in which they depend on each other for localization (Fig. 3). Because the GAP-independent localization was mainly observed under conditions with high $Tem1^{GTP}$ (i.e., in the absence of the GAP), we sought to examine whether Tem1 ($Tem1^{GTP}$) concentration plays a role in Cdc15/MEN activation.

Previous studies showed that strong overexpression of Tem1 (50-100 x) hyperactivates the MEN and bypasses the SPoC[19], suggesting the importance of Tem1 concentration in MEN activation. To assess the sensitivity of MEN activation to Tem1 concentration, we titrated the Tem1 level in the cell by introducing extra copies of the *TEM1* gene using an integrating vector (Fig. S10A). To measure MEN activity, we quantified the integrity of the SPoC by depleting both Kar9 and Dyn1 using auxin-inducible degrons to trigger spindle mispositioning[7] (Fig. 6A). Surprisingly, doubling Tem1 level with one extra copy (2x) was enough to hyperactivate the MEN such that cells were not fully prevented from exiting mitosis with a mispositioned spindle (Fig. 6A, ~40% SPoC defective). Cells with three extra copies (4x) were 95% SPoC defective (Fig. 6A). Furthermore, the time to exit mitosis in cells with mispositioned spindles decreased as Tem1 level was increased (Fig. 6B) revealing a dose-dependent relationship between Tem1 ($Tem1^{GTP}$) level and MEN hyperactivation. Conversely, reducing Tem1 levels by 50% with a heterozygous deletion in diploid cells delayed exit from mitosis (Fig. 6C), presumably due to less efficient MEN activation (Fig. S10C, reduced dSPB localization for Tem1). These results demonstrate that Cdc15 (MEN) activation is sensitive to Tem1 ($Tem1^{GTP}$) concentration.

SPB localization creates a high effective concentration of Tem1 for Cdc15 activation.

Given the effect of Tem1 concentration in MEN activation and the drastic size difference between SPB and the cell, we hypothesized that SPB localization serves as a mechanism to concentrate Tem1 for Cdc15 activation. Cdc15 has been shown to form dimers (or multimers)[30] and due to an avidity effect could be sensitive to local concentrations of Tem1. Encouragingly, we found that tethering Tem1 to other components of the SPB outer plaque such as Nud1 and Spc72 shows a similar rescuing effect for the GDP-locked *tem1T34A* as tethering to Cnm67 (Fig. 6D), ruling out the requirement for a specific SPB location/receptor for Tem1 to function.

If SPB localization is key, then concentrating Tem1 at a different site should fail to activate the MEN. Tethering Tem1 to the outer membrane of mitochondria via Tom70 failed to rescue *tem1T34A* (Fig. 6D). However, tethering Tem1 to the surface of genetically-encoded multimeric nanoparticles (GEMs, ~ 40 nm diameter)[31] fully rescued the lethality of *tem1T34A* to the same degree as tethering to the SPB (Fig. 6D). Importantly, this localization also bypassed the SPoC (Fig. S11A). Unexpectedly, Tem1T34A-coated GEMs clustered at the SPBs in a Bfa1-dependent manner (Figs. 6E & S11B), even though Tem1T34A did not localize to the SPB on its own (Fig. 2). This may be due to an avidity effect whereby the high density of Tem1T34A on GEMs compensates for the weak affinity of Tem1T34A for Bub2-Bfa1. To concentrate Tem1 away from the SPB, we repeated the GEM tethering experiment in *bfa1Δ* cells where the GEMs remained mostly in the cytosol (Fig. 6E & S11B). Under this condition, we observed the same rescuing effect for Tem1 lethal mutations defective in SPB localization (Fig. 6F). Furthermore, tethering Tem1T34A to a homo-hexamer (HOTag3)[32] instead of the GEMs (120mer), but not a tetramer (HOTag6), was sufficient to partially rescue the lethality (Fig. S11E). These results strongly support a model in which recruitment of $Tem1^{GTP}$ to the SPB primarily serves to generate a high effective concentration of Tem1 that is required for Cdc15/MEN activation and MEN signaling can be initiated elsewhere by concentrating Tem1 (Fig. 6G).

DISCUSSION

Tem1 is a noncanonical GTPase that does not function as a molecular switch.

Tem1 is a Ras-like small GTPase and has been assumed to function in a similar manner as a molecular switch. There are three key features define a canonical GTPase switch: first, there are two distinct and stable states (GTP vs GDP bound); second, only one state (typically the GTP bound state) can recruit and activate downstream effectors; lastly, the switch is controlled by changing the nucleotide state through regulatory proteins such as GAPs and GEFs. None of these features fully applies to Tem1. We showed that Tem1's high intrinsic nucleotide exchange activity is due to a lower binding affinity for guanine nucleotides (Fig. 1). As a result, $Tem1^{GDP}$ is relatively unstable *in vivo* where GTP is present in excess of GDP. Thus, Tem1 is a GEF-independent self-activating GTPase. Furthermore, we show that Tem1's effector protein Cdc15 has only a weak preference for $Tem1^{GTP}$ (Fig. 4) unlike canonical GTPase effectors (Fig. 6H). This lack of preference allows GDP-locked/apo Tem1 mutants that are correctly localized to

readily activate the MEN. Most importantly, we demonstrated that Tem1's nucleotide state ([$Tem1^{GTP}$] : [$Tem1^{GDP}$]) does not change upon MEN activation (Fig. 5). Instead, it is the localization of Tem1 that is the key change that responds to spindle position. Our results strongly suggest that Tem1 does not function as a molecular switch like Ras and is instead regulated by a noncanonical mechanism where Tem1's nucleotide cycle is used to establish a concentration difference in the cell (Fig. 6G, S8).

Tem1 is not the first small GTPase reported to have high intrinsic nucleotide exchange activity. RABL2, a Rab-like small GTPase important for ciliary assembly and function, also undergoes GEF-independent intrinsic nucleotide exchange due to a low-micromolar binding affinity for guanine nucleotides[33]. Intriguingly, RABL2 localizes to the base of primary cilia (mother centriole) in a GTP dependent manner[33,34] resembling Tem1's GTP specific localization to the SPB. Together with additional examples identified previously, these GEF-independent small GTPases form a new class of GTPases that share the feature of low binding affinity towards guanine nucleotides. Unlike Tem1, it appears that RABL2 still functions via a switch mechanism to regulate effector binding[33] suggesting that high intrinsic nucleotide exchange activity does not correlate with non-switch mechanism. On the other hand, regulation of small GTPases via protein degradation (rather than changing nucleotide states) has been reported for the oncogene RIT1 in mice[35] and flies[36] and the cytoskeleton regulator RhoB in quiescent endothelium[37] but their effector proteins still require the GTP bound form. Collectively, Tem1 represents a novel example of small GTPases that functions via a non-switch mechanism regulated by localization.

SPoC regulates the MEN by modulating effective Tem1 concentration.

We propose a new model for Tem1 regulation and SPoC that is based on localization and concentration (Fig. 6G-H). Tem1's GAP, Bub2-Bfa1, is constitutively active and keeps cellular $Tem1^{GTP}$ level low to prevent Tem1-Cdc15 interaction in the cytoplasm. Under this condition, Tem1 could only reach sufficient effective concentration to interact with Cdc15 by localizing to the SPB thus coupling MEN activation to Tem1 localization. Perturbations that increase cellular effective concentration of Tem1 either by overexpression, defective GTP hydrolysis (such as GAP mutant *bub2Δ* or *bfa1Δ*), or local clustering (tethering to GEMs) lead to Tem1-Cdc15 interaction in the cytoplasm thus bypassing the requirement of SPB localization.

SPoC further couples SPB localization of Tem1 to spindle position by regulating the GAP localization. This is achieved, at least in part, through the inhibitory zone protein Kin4 that actively removes the GAP complex from SPB that remain in the mother compartment by phosphorylating Bfa1. When the spindle is correctly positioned, the dSPB escapes the inhibitory zone leading to the accumulation of the GAP and thus Tem1 to trigger MEN activation. However, if the spindle is mispositioned and both SPBs remain in the mother cell, SPB localization of the GAP and Tem1 is inhibited, keeping Cdc15 and the MEN inactive. Decoupling SPB localization from spindle position by either tethering Tem1 or the GAP to the SPB compromises the SPoC. In addition, any perturbation that bypasses the requirement of Tem1 SPB localization for MEN activation as discussed above also leads to defective SPoC. Finally, Tem1 is imported into the nucleus for degradation after exit from mitosis[38] (Fig. S2E-F) which facilitates MEN inactivation and resets Tem1 concentration for the following cell cycle.

It is still an open question how Tem1-Cdc15 interaction leads to Cdc15 activation. Given our observation of the GAP-independent SPB localization of Tem1 and Cdc15 (Fig. 3) and the SPB component Nud1 being the scaffold for Cdc15, we favor a model in which Tem1-Cdc15 complex formation activates Cdc15 by promoting a form of Cdc15 capable of localizing to the SPB. This could explain the previous finding that tethering Tem1 to the plasma membrane (PM) in the absence of the GAP inhibits MEN activation[18]. PM tethering sequesters Tem1 and thus Cdc15 and would prevent phosphorylation of Nud1 by Cdc15. Similar effect might be at play when we tethered Tem1 to the mitochondria surface which failed to rescue *tem1T34A.* In contrast, when we tethered Tem1T34A to GEMs which are free to diffuse in the cytoplasm in the absence of the GAP, activated Cdc15 (presumably in complex with Tem1T34A on the surface of GEMs) localizes to the SPB (Fig. S11C-D) and brings Tem1T34A coated GEMs to the SPB as well (Fig. S11B).

Additional cell cycle regulation on MEN activation.

Our new model for Tem1 regulation explains how SPoC controls MEN activation in response to spindle position. However, Tem1 already localizes to the dSPB in metaphase when the MEN is supposed to be inactive, albeit at a lower level (~50%) than in anaphase when the MEN is activated (Fig. 3A). Notably, Cdc15 does not localize to the SPB until anaphase (Fig. 3A). What is preventing Tem1 from interacting and activating Cdc15 in metaphase? Given the sensitivity of

MEN activation to Tem1 concentration (Fig. 6A-C), one possibility is that the two-fold concentration difference of SPB-localized Tem1 observed between metaphase and anaphase is enough to generate different outcomes for Cdc15 activation. However, in diploid yeast with only one copy of *TEM1*, where SPB-localized Tem1 is reduced by ~50% in anaphase (Fig. S10C), MEN activation is not prevented as these cells proceed to exit from mitosis with only a ~3-min delay (Fig. 6C).

Another more plausible explanation is that there is an additional regulation of the Tem1-Cdc15 interaction that is cell-cycle dependent. It appears that in metaphase, SPB localized Tem1, although above the threshold effective concentration for Tem1-Cdc15 complex formation, is prevented from interacting with Cdc15. This inhibition is removed in anaphase to promote Cdc15 activation. As Tem1 is recruited to the SPB by Bub2-Bfa1 in metaphase (Fig. 3) and Bfa1 interacts with Tem1 on its own in a different manner than in the GAP complex (Fig. 4H), we propose that the likely candidate for the inhibitor of Tem1-Cdc15 interaction is Bfa1. In support of this hypothesis, overexpression of Bfa1 without its partner Bub2, arrests cells in anaphase[39,40], presumably through inhibiting Tem1-Cdc15 interaction.

The cell cycle regulator polo-like kinase Cdc5 phosphorylates Bfa1[14,41]. This phosphorylation has been proposed to inactivate the GAP to give rise to $Tem1^{GTP}$ and MEN activation[14]. Our results argue against this model as the GAP remains active in anaphase and Tem1's nucleotide state does not change upon MEN activation. Given that Cdc5 does not localize to the cytoplasmic facing SPB outer plaque (where Bub2-Bfa1 localizes) until anaphase[42], we propose that Cdc5, instead of regulating GAP activity, could be the cell-cycle regulator that removes the Bfa1 inhibition of Tem1-Cdc15 interaction. Cdc5 has been shown to regulate Cdc15 activation independent of Tem1[43] and our previous study revealed that Cdc5 regulates Dbf2-Mob1's access to its substrate Net1/Cfi1[44]. So, in essence, Cdc5 regulates MEN signaling at every step of the pathway to ensure that MEN activation is cell-cycle restricted.

The role of Tem1's GTP/GDP cycle.

Given that the key mode of regulation for Tem1 is by changing local concentration, why does the system need a GTPase? In other words, what additional benefit might the GTP/GDP cycle provide for Tem1 regulation? Although Cdc15 has a relatively weak preference for GTP bound Tem1, $Tem1^{GTP}$ still interacts and activates Cdc15 much more efficiently. The GTP/GDP cycle

thus provides an additional layer of concentration control to establish a concentration difference in the cell which prevents Cdc15 activation in the cytoplasm while primed for prompt MEN activation at the SPB. Our results titrating Tem1 level (Fig. 6A-C) indicates that *S. cerevisiae* cells operate with an optimum Tem1 concentration balancing the speed of mitotic exit and the necessary accuracy required for the checkpoint: increasing Tem1 level by just one extra copy hyperactivates the MEN and comprises the SPoC while lowering Tem1 level by 50% slows exit from mitosis.

Localization/concentration-based signaling mechanism.

It is intriguing that Tem1 does not function as a molecular switch like canonical small GTPases. What might be the selection pressure that favors the localization/concentration-based signaling mechanism for Tem1? Compared to chemical inputs (e.g., presence of nutrients or growth factors), sensing a spatial cue (i.e., spindle position) is a much more complex task that might necessitate a localization-based signaling mechanism. However, the spindle-position coupled localization regulation occurs at the level of the GAP, Tem1's anchor at the SPB, not Tem1 itself. Thus, it is not inconceivable for Tem1 to still function via a switch mechanism as previously assumed.

We speculate that one source of selection pressure might be Tem1's sole effector protein Cdc15. We show that surprisingly Cdc15 has a relatively weak preference for $Tem1^{GTP}$ and can be activated by GDP-locked mutant Tem1T34A at high effective concentration (tethered to SPB or GEMs). The lack of strong specificity for GTP-bound Tem1 likely poses a challenge for Tem1 to function as a binary switch. We do not yet know why Cdc15 does not behave like a canonical GTPase effector protein, but the observation that Cdc15 activation in meiosis does not depend on Tem1[45] suggests that there might be additional selection pressures on Cdc15 besides serving as an effector for Tem1. Another factor might be the speed to complete mitosis. Although Tem1 has a relatively high intrinsic nucleotide exchange rate, it still takes minutes for Tem1 to exchange GDP for GTP ($t_{1/2}$~2.3 min) once the GAP is inactivated (presumably through phosphorylation). In contrast, changing localization and binding mode of Bfa1 for Tem1 by phosphorylation is more direct and can be much faster thus providing a fitness advantage.

The localization/concentration model we described for Tem1 could be a general mechanism applicable to other localization-based signaling scenarios such as DNA damage

response[46] and kinetochore assembly[47]. The key requirement for this mechanism is a downstream binding partner (often dimetric/multimeric) that is sensitive to local concentrations of the upstream signaling molecules (due to the avidity effect). A related version of this mechanism is to modulate local concentration not by changing localization but through phase separation which has been observed for several different membrane receptor signaling pathways[48]. It is also worth noting that even for Ras, the classic example of the molecular switch mechanism, changes in local concertation through clustering at the membrane have been observed and proposed to play an important role in signaling[49]. Together with our findings for Tem1, these examples highlight that changing local/effective concentrations of signaling molecules is an important mechanism widely utilized in cell signaling.

ACKNOWLEDGEMENTS

We thank E Unal (Berkeley, USA), J Haber (Waltham, USA), T Schwartz (Cambridge, USA), A Keating (Cambridge, USA), F Monje-Casas (Sevilla, Spain), S Piatti (Montpellier, France), and L Holt (New York, USA) for strains and reagents; A Murray and D Lew for their critical reading of the manuscript. This work was supported by National Institute of General Medical Science (K99GM140212 to XZ) and the Eunice Kennedy Shriver National Institute of Child Health and Human Development (HD085866 to AA). AA and SB were also investigators of the Howard Hughes Medical Institute.

AUTHOR CONTRIBUTIONS

X.Z. and A.A. conceived the study. X.Z. performed all experiments. S.Y.W. generated Tem1 and Bub2 point mutants. X.Z. wrote the manuscript with input from S.P.B..

COMPETING INTERESTS

The authors declare no competing interests.

MATERIALS AND METHODS

Construction of Yeast strains and plasmids

All *Saccharomyces cerevisiae* yeast strains used in this study are derivatives of W303 (A2587) and are listed in Table S1. All plasmids used in this study are listed in Table S2. Yeast cells were cultured in standard YEP media (1% yeast extract, 2% peptone) with 2% D-glucose, or in standard Synthetic Complete media (SC) with 2% D-glucose. Cells were cultured at 25°C unless noted otherwise. C-terminal fusions and deletions were constructed using standard PCR-based methods. N-terminal tagging and point mutations of Tem1 and Bub2 were introduced at the endogenous locus using Cas9-mediated gene editing as described previously[44,50]. Successfully edited clones were checked by PCR and sequencing. Point mutations in GFP and small insertions in the tagging plasmids were introduced via Q5 site-directed mutagenesis. GFP and RFP (mCherry) nanobodies (GBP and RBP) were synthesized as gBlocks and inserted into tagging plasmids via Gibson assembly.

Purification of Tem1 and biotinylated Tem1

Recombinant Tem1 was expressed as a 14xHis-SUMO fusion (p2579) in *Escherichia coli* Rosetta2(DE3) cells. Protein production was induced with 0.3 mM IPTG at 14 °C for 16-20 hours. Cells were collected by centrifugation at 6,000 x g, resuspended in lysis buffer (50 mM HEPES, pH 8.0, 500 mM NaCl, 2 mM $MgCl_2$, 25 mM imidazole, 3 mM 2-mercaptoethanol (βME)) supplemented with cOmplete™ EDTA free protease inhibitor cocktail, treated with lysozyme for 30 mins at 4 °C followed by sonication. The lysate was cleared by centrifugation at 16,000 x g for 30 min. The soluble fraction was incubated with Ni-NTA agarose (QIAGEN) for 1 hour at 4 °C. The resin was washed with lysis buffer and transferred to low imidazole buffer (20 mM HEPES pH 8.0, 100 mM NaCl, 100 mM imidazole, 2 mM $MgCl_2$) along with 2.5 µg SENP protease (gift from T. Schwartz's lab[51]) and incubated at 4 °C overnight. Then the flow through containing the cleaved Tem1 was collected along with a 2 CV wash with low imidazole buffer and loaded onto a Mono S column equilibrated with buffer A (20 mM HEPES pH 8.0, 50 mM NaCl, 5 mM $MgCl_2$, 10% glycerol, 1 mM DTT). After washing with buffer A, Tem1 was eluted with a linear gradient from 0 to 100% buffer B (20 mM HEPES pH 8.0, 1 M NaCl, 5 mM $MgCl_2$, 10% glycerol, 1 mM DTT) in 20 CV. To make apo-Tem1, buffer EDTA (20 mM HEPES

pH 8.0, 50 mM NaCl, 5 mM EDTA, 10% glycerol, 1 mM DTT) was used before elution to remove nucleotides bound to Tem1. Tem1 peak fractions were pooled and concentrated.

To generate biotinylated Tem1, Tem1 was expressed as a AviTag-6xHis fusion together with BirA (p3034, based on pDW363[52]) in *Escherichia coli* Rosetta2(DE3) cells. Protein production was induced with 0.5 mM IPTG at 16 °C in 1L LB supplemented with 15 mg biotin for 16-20 hours. Cells were collected and process as described above, and the soluble fraction was incubated with Ni-NTA agarose (QIAGEN) for 1 hour at 4 °C. The resin was washed with lysis buffer followed by low imidazole buffer (20 mM HEPES pH 8.0, 100 mM NaCl, 25 mM imidazole, 5 mM $MgCl_2$) and biotinylated Tem1 was eluted with high imidazole buffer (20 mM HEPES pH 8.0, 100 mM NaCl, 250 mM imidazole, 5 mM $MgCl_2$) and loaded onto a Mono S column for additional purification (see above). Tem1 peak fractions were pooled and concentrated.

GTPase assay

GTP hydrolysis was measured for recombinant Tem1 with [α-^{32}P]-GTP. Tem1 (3.3 μM final concentration) was mixed with GTP (33 μM final) supplemented with 5 μCi [α-^{32}P]-GTP (PerkinElmer) in the reaction buffer (20 mM HEPES pH 7.5, 25 mM NaCl, 5 mM $MgCl_2$) on ice and the reaction was initiated by shifting to 30 ºC. At indicated time intervals, 2 μl reaction was removed and quenched with quench buffer (50 mM EDTA, 2% SDS) and analyzed via thin layer chromatography (TLC) on PEI-cellulose plates (Millipore sigma 105579). The plates were developed in 0.75M KH_2PO_4 (pH 3.5) and dried plates were exposed to storage phosphor screens overnight and scanned on a Typhoon phosphorimager (Cytiva). It is worth noting that when optimizing assay conditions, we found that EDTA which is often included in GTPase assays for small GTPase to increase nucleotide exchange or turnover did not make a difference in the rate of GTP hydrolysis for Tem1, consistent with Tem1's high intrinsic nucleotide exchange rate.

Nucleotide exchange and binding assay

To load Tem1 with fluorescently labeled nucleotides (i.e., MANT-GDP) for nucleotide exchange assays, recombinant Tem1 was first diluted in Tem1 dilution buffer (20 mM HEPES pH 7.5, 100 mM NaCl, 5mM $MgCl_2$, 10% glycerol, 0.2 mg/ml BSA, 2 mM DTT) to 10 μM and mixed with equal volume of 400 nM MANT-GDP or MANT-GTP/GTPγS in Tem1 binding buffer (20 mM

HEPES pH 7.5, 100 mM NaCl, 5mM $MgCl_2$). The mixture was incubated for at least 10 minutes at room temperature to reach equilibrium and then kept on ice. Three technical replicates of 18 µl MANT-GDP/GTP/GTPγS loaded Tem1 mixture were plated in a black 384-well nonbinding microplate (Greiner Bio-One) and read in a SpectraMax ID5 plate reader (Molecular Dynamics) at 30 ºC. To initiate nucleotide exchange, 2 µl of 10 mM unlabeled nucleotide (i.e., GTP) was added (1 mM final concentration) and readings were taken at 30s interval with 355 nm excitation and 448 nm emission. k_{obs} was measured by fitting a single exponential decay after background subtraction.

To measure binding affinities, apo-Tem1 was diluted with Tem1 dilution buffer first to 40 µM then 2-fold serial diluted 10 times with the dilution buffer. Equal volumes of 400 nM MANT-GDP or MANT-GTPγS in Tem1 binding buffer were mixed with the apo-Tem1 dilution series and 15 µl of each mixture was placed in a black 384-well nonbinding microplate (Greiner Bio-One) and read in a SpectraMax ID5 plate reader (Molecular Dynamics) after 30 minutes incubation at 30 ºC. Three independent dilutions were performed for each nucleotide conditions. K_D was measured by fitting a quadratic equation:

$y = y_{max}\left(L + P + K_D - \sqrt{(L + P + K_D)^2 - 4LP}\right)/2L$, where y_{max} is the maximum fluorescence signal at saturated binding, L is the total ligand concentration (MANT-GDP/GTPγS, 0.2 µM), P is total Tem1 concentration.

Microscopy and image analysis

For live-cell microscopy, cells were imaged on agarose pads (2% agarose in SC medium + 2% glucose, unless otherwise noted) affixed to a glass slide and covered with a coverslip. Imaging was performed on a DeltaVision Elite platform (GE Healthcare Bio-Sciences) with an InsightSSI solid state light source, an UltimateFocus hardware autofocus system and a model IX-71, Olympus microscope controlled by SoftWoRx software. A 60x Plan APO 1.42NA objective and CoolSNAP HQ2 camera were used for image acquisition. For each time point, 8 *z* sections with 0.75 µm spacing were collect for each channel and were deconvolved. Maximum projections of the deconvolved *z* stack were used for fluorescence quantification.

Image analysis was performed with custom scripts in MATLAB as described previously. First, yeast cells were segmented and tracked through time using the bright-field image stacks.

Next, fluorescence images of cell cycle markers (such as Spc42 or NLS) were segmented and tracked based on cell segmentation. Appearance of a cell cycle marker in a cell during the acquisition period was used to identify buds (daughter cells) and cell division events. Tracking of the cell cycle markers that migrated into the buds were used to identify the corresponding mother cells. Finally, for each division event identified, localization of the target protein at regions defined by the cell cycle markers was quantified.

For localization at the SPBs (I_{SPB}), maximum intensity of the target protein at SPBs (based on segmentation of Spc42) was used given that the size of SPBs (~100 nm) is within the diffraction limit of light microscopy. To calculate the relative enrichment of target protein at the SPB, intensities were normalized to the median intensity in the cytosol: $I_{SPB}/I_{cytosol} - 1$. Single cell traces were aligned based on the timing of anaphase onset or the movement of a SPB into the bud as indicated in figures, and averaged. 95% confidence intervals were calculated as $\mu \pm 1.96 * \sigma/\sqrt{n}$, where μ and σ denote the mean and standard deviation respectively and n is the number of cells measured.

Spotting assays

Tem1 mutants were constructed in the native locus with CRISPR in y3059 carrying a hyperactive Dbf2. Correct mutants were then crossed with y2892 (*tem1* knockout carrying a URA3-based CEN covering plasmid expressing wild-type Tem1) to generate strains with Tem1 mutants and the covering plasmid. Additional alleles tested were also introduced via cross. For spotting assays, these strains were grown in YPD overnight and diluted to OD 0.2 in YPD and grow for at least one doubling at room temperature. 5-fold serial dilutions were made for each culture starting from OD 0.2 and 4 µl were spotted onto YPD or plates with 5'-fluoroorotic acid (5-FOA) which selects cells that are viable after losing the URA3 covering plasmid.

Immunoblot analysis

Log-phase cultures of cells grown in YEP + 2% glucose were harvested and treated with 5% TCA at 4°C overnight. TCA treated cell pellets were washed with acetone, air dried, and resuspended in lysis buffer (10 mM Tris, 1 mM EDTA, 2.75 mM DTT, pH = 8). Cells were lysed by bead-beating using a Multivortexer (max speed, 20 minutes) and glass beads at 4°C and followed by boiling in SDS PAGE protein loading buffer for 5 minutes. Lysates were clarified

by centrifugation and were resolved with NuPAGE 4-12% Bis-Tris protein gel (Thermo Fisher Scientific) prior to transfer onto nitrocellulose membranes. Tem1 was detected with an anti-Tem1 antibody generated in rabbit against the peptide CKKLTIPEINEIGDPLLIYKHL[19] at a 1:300 dilution. GFP was detected using an anti-GFP antibody (Clontech, JL-8) at a 1:1000 dilution. Myc tags were detected using an anti-Myc antibody (abcam, 9E10) at a 1:500 dilution. V5 tags were detected using an anti-V5 antibody (Invitrogen) at a 1:2000 dilution. HA tags were detected with an anti-HA.11 antibody (BioLegend) at 1:1000 dilution. Clb2 was detected using a rabbit anti-Clb2 at 1:1000 dilution. Kar2 was detected using a rabbit anti-Kar2 antiserum at a 1:200,000 dilution. DyLight 800 conjugated secondary antibodies (Cell Signaling) were used at a 1 :10,000 dilution. Blots were imaged using the ChemiDoc MP imager system (BioRad).

Co-immunoprecipitation analysis

Log-phase cultures (~ 40 OD of cells) were harvested and snap frozen in liquid nitrogen. Cell pellets were thawed in lysis buffer (50 mM Tris pH=7.5, 150mM NaCl, 1% NP40, 5mM MgCl2, 1mM DTT, supplemented with cOmplete™ EDTA free protease inhibitor and PhosSTOP™ inhibitor) and lysed via bead-beating with silica beads in a FastPrep-24™ (MP Biomedicals). Lysates were clarified by centrifugation and protein concentration in the lysates was measured with Bradford assay (Bio-Rad). 15 µl of GFP-Trap agarose (ChromoTek) was washed three times with NP40 buffer (50 mM Tris pH=7.5, 150mM NaCl, 1% NP40, 5mM MgCl2) and incubated with clarified lysates containing ~3 mg of total protein per sample for 1 hour at 4 ºC. The agarose beads were washed five times with NP40 buffer. Afterwards, the bound proteins were eluted by boiling the beads in protein loading buffer and resolved on NuPAGE 4–12% Bis-Tris protein gels (Thermo Fisher Scientific) followed by immunoblot analysis (see above).

AlphaLISA analysis

Purified biotinylated Tem1 was first diluted to 500 nM and incubated with 100 µM GTPγS or GDP in assay buffer (50 mM Tris pH=7.5, 150mM NaCl, 1% NP40, 5mM MgCl2, 1mM DTT, 1x cOmplete™ EDTA free protease inhibitor and PhosSTOP™ inhibitor, 0.1% BSA) and 3-fold serial diluted. Equal volume of 100 µg/ml (5x final concentration) Alphascreen Streptavidin Donor beads (PerkinElmer 6760002S) diluted in assay buffer were added and incubated with nucleotide loaded Tem1 for 1 hour at room temperature in the dark. Log-phase cultures (~ 10

OD of cells) containing eGFP tagged Bub2/Bfa1/Cdc15 were harvested and snap frozen in liquid nitrogen. Cell pellets were processed as described for co-immunoprecipitation assays and diluted to 3 mg/ml total protein concentration with lysis buffer. 5 µl lysate was added to each 384 well Alpha plates (PerkinElmer) together with 10 µl Tem1 coated donor beads and 10 µl 50 µg/µl AlphaLISA Anti-GFP Acceptor Beads (PerkinElmer AL133C) diluted in assay buffer. The plate was incubated for 4-6 hours at 4 ºC and read using a M1000 plate reader (Tecan) with the default AlphaScreen settings at room temperature. For the competition assays with unlabeled Tem1, 0.5 nM and 5 nM final concentration of biotinylated Tem1 were used for the GTPγS and GDP binding assays respectively.

FRAP analysis

FRAP analysis was performed on a DeltaVision-OMX Super-Resolution Microscope (Applied Precision, GE Healthcare Bio-Sciences) using a 60x oil objective and a 488 nm laser adjusted to bleach an area of approximately 0.5 µm in radius. Two prebleach images were acquired followed by a laser pulse (50% intensity) of 0.02 s duration and postbleach images were acquired at 1 s/frame for 60 s. Images at each time points were maximum projections of 5 *z* stacks with 0.5 µm spacing. Images were analyzed with a custom MATLAB script. After subtracting the background, fluorescence intensities in the cytosol, $I_{cytosol}(t)$, and at the SPB, $I_{SPB}(t)$ were measured after segmenting the cell and SPBs. Photobleaching was corrected by normalizing $I_{SPB}(t)$ with $I_{cytosol}(t)$, $I_{SPB_norm}(t) = I_{SPB}(t) / I_{cytosol}(t)$. Double normalization for FRAP was calculated to scale the photobleaching effect between 0 and 1: $I_{SPB_FRAP}(t) = [I_{SPB_norm}(t) - I_{SPB_norm}(0)] / [I_{SPB_norm}(pre) - I_{SPB_norm}(0)]$, where $t = 0$ is the time point (frame) right after photobleaching and $t = pre$ is the time point (frame) right before photobleaching. The double normalized FRAP curves were then fitted to a single exponential curve: $y = y_{max}\left(1 - e^{\left(-ln2/t_{1/2}\right)t}\right)$, where y_{max} is the fraction recovered while $t_{1/2}$ is the half-recovery time.

SPoC assay

Spindle mispositioning was induced by depleting both Kar9 and Dyn1 with the auxin-inducible degron system. Spindle position and checkpoint integrity was monitored with fluorescently labeled α-tubulin (GFP-Tub1 or mCherry-Tub1). Cells were imaged on agarose pads (2%

agarose in SC medium + 2% glucose + 100 μM IAA) as described in Microscopy at 5 min interval for 4 to 5 hours. Images were analyzed by scoring the following 4 categories: spindle elongated in the mother cell and the cell was arrested in anaphase with elongated spindle (1), spindle elongated in the mother cell and the cell exited mitosis with spindle disassembled in the mother cell (2), spindle elongated in the mother cell but later extended into the bud and exited mitosis with one spindle pole in the bud (3), and spindle elongated into the bud and exited mitosis with one spindle pole in the bud (4). Only categories 1&2 were used to calculate the percentages of cells arrested vs exited in mother.

Modeling Tem1's nucleotide cycle

Virtual Cell software (VCell[53,54]) version 7.5.0 was used to model Tem1's nucleotide cycle. The model, "Tem1_Bfa1" by user "xiaoxuez", can be accessed within the VCell software (available at https://vcell.org). Two compartments (cytosol and SPB) were set up for the GAP stimulated GTP hydrolysis and GEF-independent nucleotide exchange where the GAP (represented in the model as "Bfa1") was placed at SPB to simulate anaphase cells. We have also simulated metaphase cells by distributing the GAP evenly between the cytosol and SPB and found no difference in the results. Each simulation started with 25 nM $Tem1^{GTP}$ (~ 1500 molecules/cell) in the cytosol and ran for 300 s to reach steady state. The parameters used can be found in the online model and the parameters scanned are summarized in Fig. S8B.

REFERENCES

1. Wennerberg, K. The Ras superfamily at a glance. *J. Cell Sci.* **118**, 843–846 (2005).
2. Vetter, I. R. & Wittinghofer, A. The Guanine Nucleotide-Binding Switch in Three Dimensions. *Science* **294**, 1299–1304 (2001).
3. Bos, J. L., Rehmann, H. & Wittinghofer, A. GEFs and GAPs: Critical Elements in the Control of Small G Proteins. *Cell* **129**, 865–877 (2007).
4. Simanshu, D. K., Nissley, D. V. & McCormick, F. RAS Proteins and Their Regulators in Human Disease. *Cell* **170**, 17–33 (2017).
5. Guertin, D. A., Trautmann, S. & McCollum, D. Cytokinesis in Eukaryotes. *Microbiol. Mol. Biol. Rev.* **66**, 155–178 (2002).
6. Chan, L. Y. & Amon, A. Spindle Position Is Coordinated with Cell-Cycle Progression through Establishment of Mitotic Exit-Activating and -Inhibitory Zones. *Mol. Cell* **39**, 444–454 (2010).
7. Falk, J. E. *et al.* Spatial signals link exit from mitosis to spindle position. *eLife* **5**, e14036 (2016).
8. Campbell, I. W., Zhou, X. & Amon, A. The Mitotic Exit Network integrates temporal and spatial signals by distributing regulation across multiple components. *eLife* **8**, (2019).
9. Bardin, A. J., Visintin, R. & Amon, A. A Mechanism for Coupling Exit from Mitosis to Partitioning of the Nucleus. *Cell* **102**, 21–31 (2000).
10. Pereira, G., Höfken, T., Grindlay, J., Manson, C. & Schiebel, E. The Bub2p Spindle Checkpoint Links Nuclear Migration with Mitotic Exit. *Mol. Cell* **6**, 1–10 (2000).
11. Scarfone, I. *et al.* Asymmetry of the Budding Yeast Tem1 GTPase at Spindle Poles Is Required for Spindle Positioning But Not for Mitotic Exit. *PLOS Genet.* **11**, e1004938 (2015).

12. Asakawa, K., Yoshida, S., Otake, F. & Toh-e, A. A novel functional domain of Cdc15 kinase is required for its interaction with Tem1 GTPase in Saccharomyces cerevisiae. *Genetics* **157**, 1437–1450 (2001).
13. Geymonat, M. *et al.* Control of Mitotic Exit in Budding Yeast. *J. Biol. Chem.* **277**, 28439–28445 (2002).
14. Geymonat, M., Spanos, A., Walker, P. A., Johnston, L. H. & Sedgwick, S. G. *In Vitro* Regulation of Budding Yeast Bfa1/Bub2 GAP Activity by Cdc5. *J. Biol. Chem.* **278**, 14591–14594 (2003).
15. Molk, J. N. *et al.* The Differential Roles of Budding Yeast Tem1p, Cdc15p, and Bub2p Protein Dynamics in Mitotic Exit□D□V. *Mol. Biol. Cell* **15**, (2004).
16. Campbell, I. W., Zhou, X. & Amon, A. Spindle pole bodies function as signal amplifiers in the Mitotic Exit Network. *Mol. Biol. Cell* **31**, 906–916 (2020).
17. Caydasi, A. K. & Pereira, G. Spindle Alignment Regulates the Dynamic Association of Checkpoint Proteins with Yeast Spindle Pole Bodies. *Dev. Cell* **16**, 146–156 (2009).
18. Valerio-Santiago, M. & Monje-Casas, F. Tem1 localization to the spindle pole bodies is essential for mitotic exit and impairs spindle checkpoint function. *J. Cell Biol.* **192**, 599–614 (2011).
19. Chan, L. Y. & Amon, A. The protein phosphatase 2A functions in the spindle position checkpoint by regulating the checkpoint kinase Kin4. *Genes Dev.* **23**, 1639–1649 (2009).
20. Maekawa, H., Priest, C., Lechner, J., Pereira, G. & Schiebel, E. The yeast centrosome translates the positional information of the anaphase spindle into a cell cycle signal. *J. Cell Biol.* **179**, 423–436 (2007).

21. D'Aquino, K. E. *et al.* The Protein Kinase Kin4 Inhibits Exit from Mitosis in Response to Spindle Position Defects. *Mol. Cell* **19**, 223–234 (2005).

22. Pereira, G. & Schiebel, E. Kin4 Kinase Delays Mitotic Exit in Response to Spindle Alignment Defects. *Mol. Cell* **19**, 209–221 (2005).

23. Morawska, M. & Ulrich, H. D. An expanded tool kit for the auxin-inducible degron system in budding yeast. *Yeast Chichester Engl.* **30**, 341–351 (2013).

24. Geymonat, M., Spanos, A., de Bettignies, G. & Sedgwick, S. G. Lte1 contributes to Bfa1 localization rather than stimulating nucleotide exchange by Tem1. *J. Cell Biol.* **187**, 497–511 (2009).

25. Beaudet, L. *et al.* AlphaLISA immunoassays: the no-wash alternative to ELISAs for research and drug discovery. *Nat. Methods* **5**, an8–an9 (2008).

26. Humphreys, I. R. *et al.* Computed structures of core eukaryotic protein complexes. *Science* **374**, eabm4805 (2021).

27. Caydasi, A. K. *et al.* A dynamical model of the spindle position checkpoint. *Mol. Syst. Biol.* **8**, 582 (2012).

28. Jaspersen, S. L. & Morgan, D. O. Cdc14 activates Cdc15 to promote mitotic exit in budding yeast. *Curr. Biol.* **10**, 615–618 (2000).

29. Rock, J. M. *et al.* Activation of the Yeast Hippo Pathway by Phosphorylation-Dependent Assembly of Signaling Complexes. *Science* **340**, 871–875 (2013).

30. Bardin, A. J., Boselli, M. G. & Amon, A. Mitotic Exit Regulation through Distinct Domains within the Protein Kinase Cdc15. *Mol. Cell. Biol.* **23**, 5018–5030 (2003).

31. Delarue, M. *et al.* mTORC1 Controls Phase Separation and the Biophysical Properties of the Cytoplasm by Tuning Crowding. *Cell* **174**, 338-349.e20 (2018).

32. Zhang, Q. *et al.* Visualizing Dynamics of Cell Signaling In Vivo with a Phase Separation-Based Kinase Reporter. *Mol. Cell* **69**, 334-346.e4 (2018).

33. Kanie, T. *et al.* The CEP19-RABL2 GTPase Complex Binds IFT-B to Initiate Intraflagellar Transport at the Ciliary Base. *Dev. Cell* **42**, 22-36.e12 (2017).

34. Nishijima, Y. *et al.* RABL2 interacts with the intraflagellar transport-B complex and CEP19 and participates in ciliary assembly. *Mol. Biol. Cell* **28**, 1652–1666 (2017).

35. Castel, P. *et al.* RIT1 oncoproteins escape LZTR1-mediated proteolysis. *Science* **363**, 1226–1230 (2019).

36. Cuevas-Navarro, A. *et al.* Cross-species analysis of LZTR1 loss-of-function mutants demonstrates dependency to RIT1 orthologs. *eLife* **11**, e76495 (2022).

37. Podieh, F. *et al.* Differential role for rapid proteostasis in Rho GTPase-mediated control of quiescent endothelial integrity. *J. Biol. Chem.* **299**, 104593 (2023).

38. Devault, A. & Piatti, S. Downregulation of the Tem1 GTPase by Amn1 after cytokinesis involves both nuclear import and SCF-mediated degradation. *J. Cell Sci.* **134**, jcs258972 (2021).

39. Ro, H.-S., Song, S. & Lee, K. S. Bfa1 can regulate Tem1 function independently of Bub2 in the mitotic exit network of Saccharomyces cerevisiae. *Proc. Natl. Acad. Sci.* **99**, 5436–5441 (2002).

40. Whalen, J., Sniffen, C., Gartland, S., Vannini, M. & Seshan, A. Budding Yeast BFA1 Has Multiple Positive Roles in Directing Late Mitotic Events. *G3 GenesGenomesGenetics* **8**, 3397–3410 (2018).

41. Hu, F. *et al.* Regulation of the Bub2/Bfa1 GAP Complex by Cdc5 and Cell Cycle Checkpoints. *Cell* **107**, 655–665 (2001).

42. Botchkarev, V. V., Rossio, V. & Yoshida, S. The budding yeast Polo-like kinase Cdc5 is released from the nucleus during anaphase for timely mitotic exit. *Cell Cycle* **13**, 3260–3270 (2014).

43. Rock, J. M. & Amon, A. Cdc15 integrates Tem1 GTPase-mediated spatial signals with Polo kinase-mediated temporal cues to activate mitotic exit. *Genes Dev.* **25**, 1943–1954 (2011).

44. Zhou, X., Li, W., Liu, Y. & Amon, A. Cross-compartment signal propagation in the mitotic exit network. *eLife* **10**, e63645 (2021).

45. Pablo-Hernando, M. E. *et al.* Cdc15 Is Required for Spore Morphogenesis Independently of Cdc14 in *Saccharomyces cerevisiae*. *Genetics* **177**, 281–293 (2007).

46. Ruis, K., Huynh, O., Montales, K., Barr, N. A. & Michael, W. M. Delineation of a minimal topoisomerase II binding protein 1 for regulated activation of ATR at DNA double-strand breaks. *J. Biol. Chem.* **298**, (2022).

47. Sissoko, G. B., Tarasovetc, E. V., Marescal, O., Grishchuk, E. L. & Cheeseman, I. M. Higher-order protein assembly controls kinetochore formation. *Nat. Cell Biol.* **26**, 45–56 (2024).

48. Case, L. B., Ditlev, J. A. & Rosen, M. K. Regulation of Transmembrane Signaling by Phase Separation. *Annu. Rev. Biophys.* **48**, 465–494 (2019).

49. Zhou, Y. & Hancock, J. F. Ras nanoclusters: Versatile lipid-based signaling platforms. *Biochim. Biophys. Acta BBA - Mol. Cell Res.* **1853**, 841–849 (2015).

50. Anand, R., Memisoglu, G. & Haber, J. Cas9-mediated gene editing in Saccharomyces cerevisiae. *Protoc. Exch.* (2017) doi:10.1038/protex.2017.021a.

51. Nordeen, S. A., Turman, D. L. & Schwartz, T. U. Yeast Nup84-Nup133 complex structure details flexibility and reveals conservation of the membrane anchoring ALPS motif. *Nat. Commun.* **11**, 6060 (2020).

52. Tsao, K.-L., Debarbieri, B., Michel, H. & Waugh, D. S. A versatile plasmid expression vector for the production of biotinylated proteins by site-specific, enzymatic modification in *Escherichia coli*. *Gene* **169**, 59–64 (1996).

53. Schaff, J., Fink, C. C., Slepchenko, B., Carson, J. H. & Loew, L. M. A general computational framework for modeling cellular structure and function. *Biophys. J.* **73**, 1135–1146 (1997).

54. Cowan, A. E., Moraru, I. I., Schaff, J. C., Slepchenko, B. M. & Loew, L. M. Chapter 8 - Spatial Modeling of Cell Signaling Networks. in *Methods in Cell Biology* (eds. Asthagiri, A. R. & Arkin, A. P.) vol. 110 195–221 (Academic Press, 2012).

Figure 1: Tem1 is a noncanonical GTPase with high intrinsic nucleotide exchange rate.

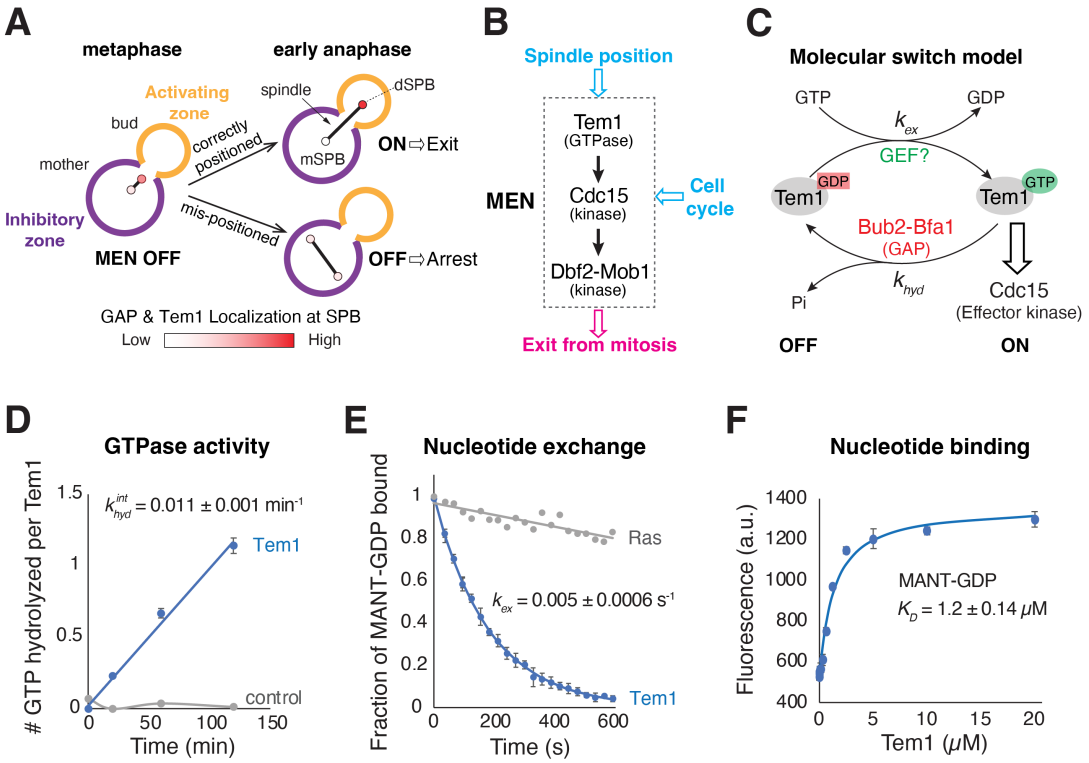

(**A**) Illustration of the spindle position checkpoint in budding yeast and localization of the MEN GTPase Tem1 and its GAP.

(**B**) Major components of the MEN and its inputs and outputs.

(**C**) Molecular switch model for Tem1.

(**D**) GTPase activity of Tem1. Recombinantly purified Tem1 was mixed with GTP and [α-^{32}P]GTP on ice and the reaction was initiated by shifting to 30 °C. Samples were taken at indicated time points and analyzed by TLC (Fig. S1B-C). Shown are the average of 3 technical replicates with a linear fit. Error bars represent ± SD.

(**E**) The rate of nucleotide exchange (MANT-GDP to GTP) for Tem1 and N-Ras. Recombinantly purified Tem1 (5 μM final) and N-Ras was first incubated with MANT-GDP (200 nM final) and the nucleotide exchange was initiated by the addition of excess GTP (1 mM). Shown are the average of 3 technical replicates with an exponential fit for Tem1 and a linear fit for N-Ras. Error bars represent ± SD.

(**F**) The binding affinity of Tem1 for MANT-GDP. 200 nM MANT-GDP was titrated with increasing amount of purified apo-Tem1. Shown are the average from 3 technical replicates with a quadratic fit for the dissociation constant (K_D). Error bars represent ± SD.

Figure 2: Nucleotide state regulates Tem1 function by controlling its localization.

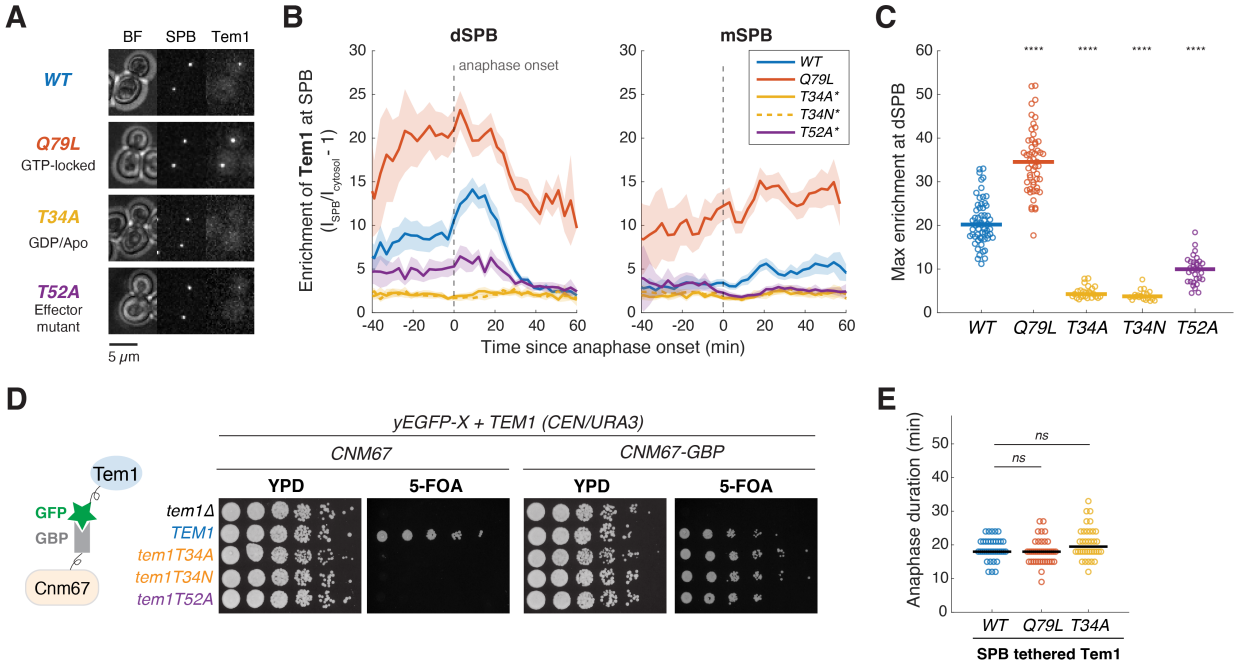

(**A-C**) Representative images and quantification of SPB localization in wild-type (y1748, n = 73 cells), GTP-locked hydrolysis mutant Q79L (y1824, n = 63 cells), GDP-locked/apo nucleotide binding mutant T34A/N (y3167/y3171, n = 29/21 cells), and effector binding mutant T52A (y3147, n = 32 cells) of Tem1. Cells expressing *tem1T34A/N* and *tem1T52A* (marked with *) were kept alive with the hyperactive *DBF2-HyA* that can rescue *tem1Δ*. Cells were grown at 25°C in SC medium + 2% glucose and imaged every 3 minutes for 4 hours. Single cell traces were aligned based on anaphase onset, as defined as spindle length > 3 μm (measured based on SPB marker Spc42-mScarlet-I), and averaged. Solid lines represent the mean, shaded areas represent 95% confidence intervals. For maximum enrichment at SPB, solid lines represent the median. ****$p < 0.0001$ by two-sided Wilcoxon rank sum test for comparing with *WT*.

(**D**) Complementation analysis of Tem1 mutants with and without tethering to the SPB via *CNM67-GBP*. 5-fold serial dilutions of strains y2891/y3202/y3203/y3204/y3214 and y3303/y3304/y3305/y3306/y3310, with the indicated *TEM1* alleles, were spotted onto plates with or without 5'-fluoroorotic acid (5-FOA) and incubated at 25°C for 2 to 3 days. The presence of 5-FOA selects cells that are viable after losing the *TEM1 (URA3/CEN)* plasmid. GBP = GFP binding protein.

(**E**) Distribution of anaphase duration for different *yEGFP-TEM1* alleles in the presence of *CNM67-GBP* (y3289, y3287, and y3291; *n* =46, 43, and 47 cells respectively) measured using the SPB marker Spc42-mScarlet-I. Cells were grown at 25°C in SC medium + 2% glucose and imaged every 3 minutes for 4 hours. Solid lines represent the median.

Figure 3: Localization of Tem1 to the SPB depends on its GAP and effector.

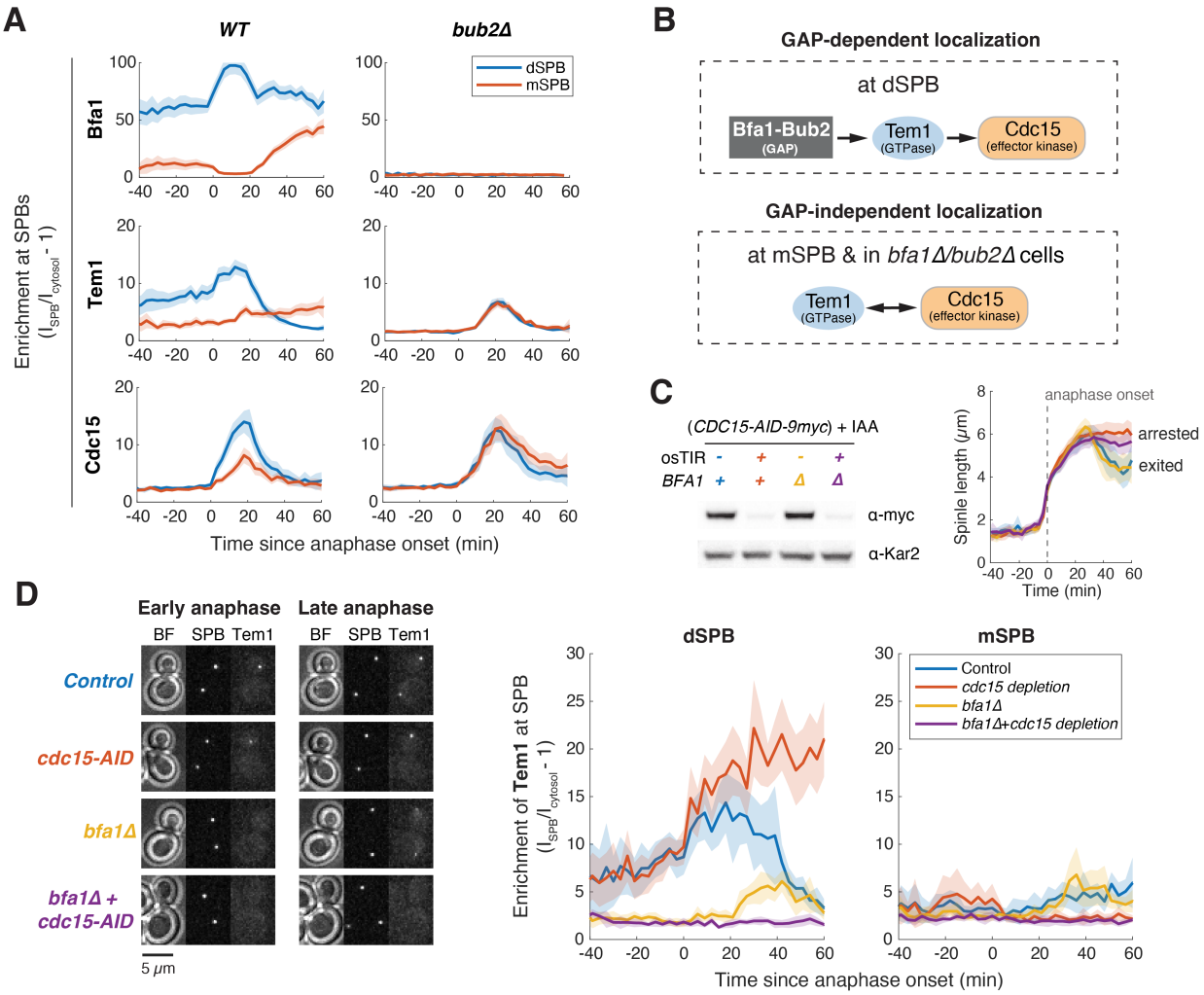

(**A**) Comparison of SPB localization for Bfa1, Tem1 and Cdc15 with or without *BUB2*. Cells with the indicated *BUB2* alleles (columns) and yEGFP-labeled proteins (rows) were grown at 25 °C in SC medium + 2% glucose and imaged every 3 minutes for 4 hours. Strains imaged were y1374 (Bfa1-yEGFP, *n* = 104 cells), y3099 (Bfa1-yEGFP in *bub2Δ*, *n* = 17 cells), y1748 (yEGFP-Tem1, *n* = 65 cells), y1929 (yEGFP-Tem1 in *bub2Δ*, *n* = 72 cells), y1275 (Cdc15-yEGFP, *n* = 79 cells), and y1693 (Cdc15-yEGFP in *bub2Δ*, *n* = 76 cells).

(**B**) Dependency of SPB localization for two different modes of localization patterns.

(**C**) Cdc15 is efficiently depleted with the auxin-inducible degron (*cdc15-AID*). Cells with the indicated genotypes (y3229 (*osTIR-/BFA1*), y3224 (*osTIR+/BFA1*), y3228 (*osTIR-/bfa1Δ*), y3223 (*osTIR+/ bfa1Δ*)) were grown at 25 °C in SC medium + 2% glucose + 200 μM IAA for 2 hours before harvesting for Western blot analysis (left). Anaphase progression (right) was

monitored in these cells by measuring spindle length (distance between two SPBs). Cells with Cdc15 depleted arrested in anaphase with elongated spindles whereas non-depleted cells disassembled their spindle (as indicated by the shortening of the distance between SPBs in late anaphase) to exit from mitosis.

(**D**) Representative images (left) and quantification (right) of Tem1 localization at the SPB with or without depleting Cdc15 (*cdc15-AID* +/- *osTIR*) in the presence or absence of *BFA1*. Cells of y3229 (Tem1 control, n = 16 cells), y3224 (Tem1 with Cdc15 depletion, n = 16 cells), y3228 (Tem1 in *bfa1Δ*, n = 12 cells), y3223 (Tem1 in *bfa1Δ* with Cdc15 depletion, n = 10 cells), y3231 (Tem1Q79L control, n = 18 cells), y3226 (Tem1Q79L with Cdc15 depletion, n = 14 cells), y3230 (Tem1Q79L in *bfa1Δ*, n = 16 cells), and y3225 (Tem1Q79L in *bfa1Δ* with Cdc15 depletion, n = 17 cells) were grown at 25 °C in SC medium + 2% glucose + 200 μM auxin IAA and imaged every 3 minutes for 4 hours.

For all graphs, single cell traces were aligned based on anaphase onset, as defined as spindle length > 3 μm (measured based on SPB marker Spc42-mScarlet-I), and averaged. Solid lines represent the average. Shaded areas represent 95% confidence intervals.

Figure 4: The GAP complex Bub2-Bfa1 preferentially binds Tem1^{GTP}.

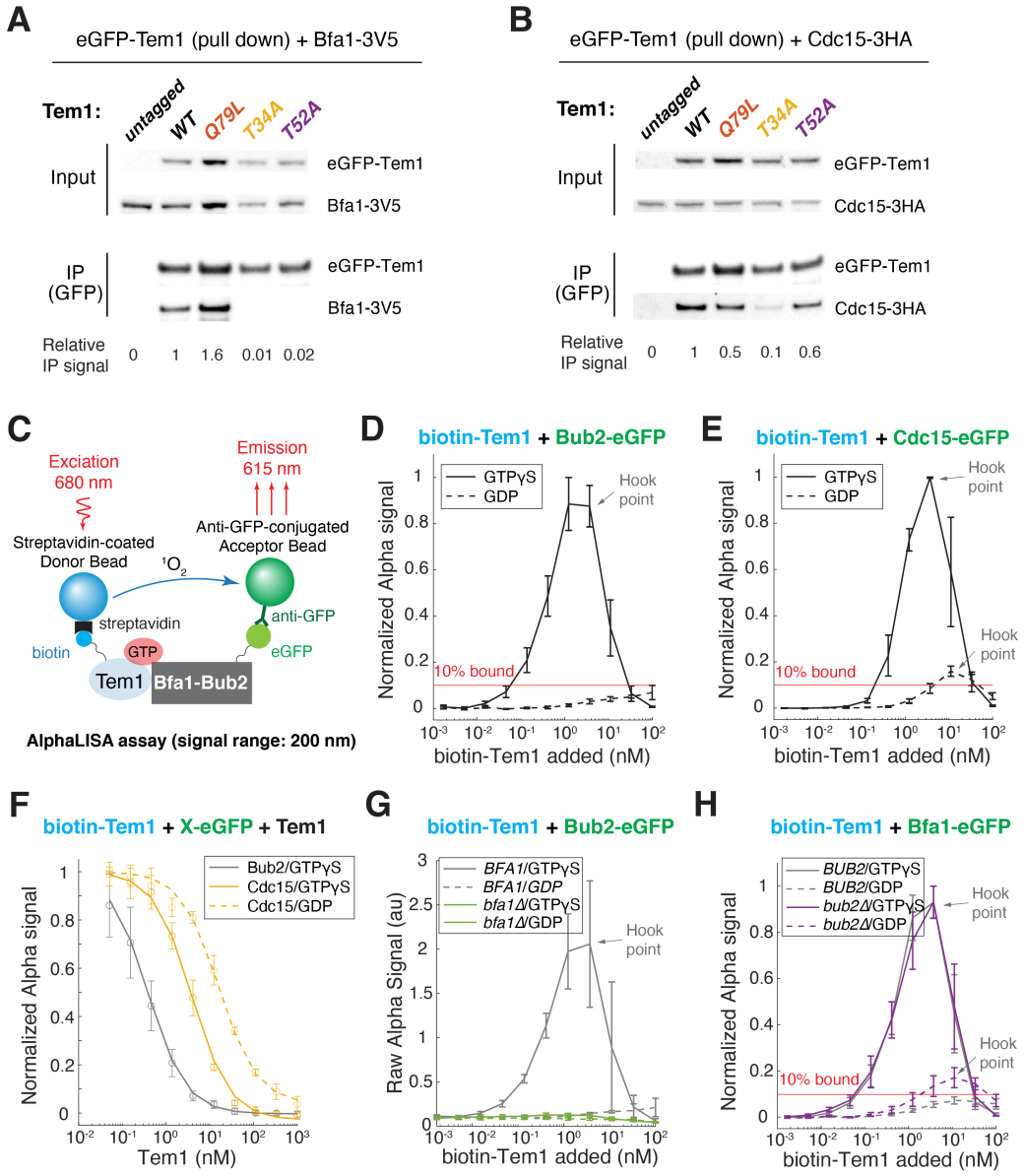

(**A-B**) Interaction between different Tem1 mutants and the GAP complex (A) or Cdc15 (B) via co-immunoprecipitation. yEGFP-Tem1 was immunoprecipitated from exponentially grown cells of the indicated genotypes (y3461/y3452/y3472/y3457/y3456 or y2761/y2885/y2886/y3209/y3208) and the presence of Bfa1-3V5 or Cdc15-3HA were analyzed by Western blot analysis.

(**C**) Illustration of the hybrid AlphaLISA assay used in this study. Recombinant biotinylated Tem1 were incubated together with cell lysate with eGFP tagged binding partners in the presence

of GTPγS or GDP. The interaction was monitored with streptavidin coated Alpha donor beads and anti-GFP conjugated accepter beads.

(**D-E**) Interaction between recombinant biotinylated Tem1 and eGFP tagged Bub2 (D) or Cdc15 (E) in lysate monitored by AlphaLISA. Diluted lysate of y1378 (Bub2-eGFP) or y1275 (Cdc15-eGFP) were incubated with different concentrations of recombinant biotinylated Tem1 in the presence of GTPγS or GDP. The Alpha signals were normalized to the maximum signal of each sample in the GTPγS condition. Black lines represent the average of three biological replicates and error bars denote standard deviation (SD). The Hook point is when the biotin-Tem1 added exceeds the binding capacity of the Alpha Donor beads which results in a competition between biotin-Tem1 in solution and on beads for binding. Red line indicates 10% of the available eGFP tagged protein (maximum binding capacity defined by the GTPγS condition) were bound by biotin-Tem1 on beads.

(**F**) Dissociation constant of Tem1 binding to Cdc15 and the GAP estimated by a competition binding assay. Diluted lysate of y1378 (Bub2-eGFP) or y1275 (Cdc15-eGFP) were incubated with a fixed amount of biotinylated Tem1 with different concentrations of unlabeled Tem1 in the presence of GTPγS or GDP. Signal for Bub2-eGFP with GDP was too low to be quantified reliably. The Alpha signals were double normalized to the signal without competing Tem1 (normalized signal = 1) and without biotin-Tem1 (normalized signal = 0). Lines represent the average of three biological replicates and error bars denote SD.

(**G-H**) Interaction between biotinylated Tem1 and eGFP tagged Bub2 (G) or Bfa1 (H). Diluted lysate of y1374 (Bfa1-eGFP), y1378 (Bub2-eGFP), y3099 (Bfa1-eGFP in *bub2Δ*), or y3632 (Bub2-eGFP in *bfa1Δ*) were incubated with different concentrations of biotinylated Tem1 in the presence of GTPγS or GDP, and the interaction was monitored with AlphaLISA. Lines represent the average of three biological replicates and error bars denote SD.

Figure 5: Tem1's nucleotide state does not change upon MEN activation.

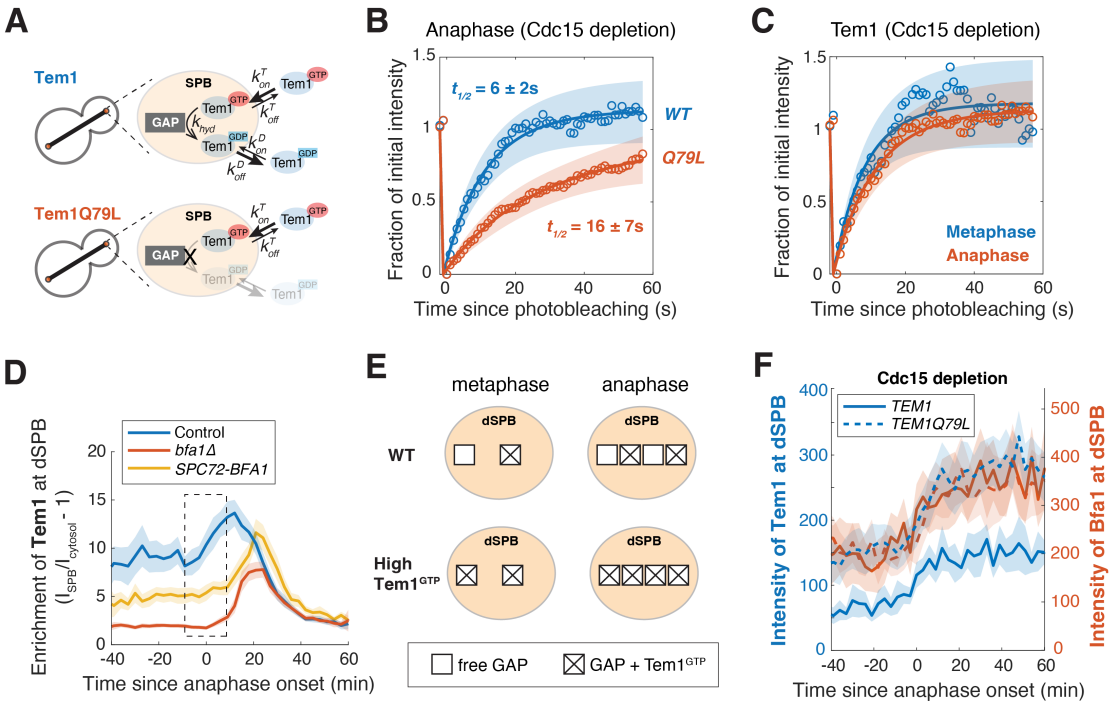

(**A**) Illustration of the different routes for Tem1 and the GTP-locked Tem1Q79L at dSPB. Once $Tem1^{GTP}$ is recruited to the dSPB by the GAP, its departure can occur either via $Tem1^{GTP}$ dissociation (k_{off}^{T}) or GAP-stimulated GTP hydrolysis (k_{hyd}) followed by dissociation (k_{off}^{D}). Assuming $k_{off}^{D} >> k_{hyd}$, the residence time of Tem1 at the dSPB ($t_{1/2}^{Tem1}$) is set by the sum of two rates: $t_{1/2}^{Tem1} = \ln 2/(k_{off}^{T} + k_{hyd})$. For Tem1Q79L, its residence time ($t_{1/2}^{Tem1Q79L}$) is simply $t_{1/2}^{Tem1Q79L} = \ln 2/k_{off}^{T}$ assuming that $Tem1^{GTP}$ and Tem1Q79L dissociate at similar rates.

(**B**) FRAP analysis of Tem1 and TemQ79L at dSPB in anaphase. Cells of y3900 (*TEM1*, n = 9 cells) and y3903 (*TEM1Q79L*, n = 15 cells) were grown and imaged at room temperature in SC medium + 2% glucose + 100 µM IAA. Circles represent the average normalized fluorescence intensities after correcting for photo-bleaching during acquisition. Solid lines are the average fit and shaded areas represent SD. Half recovery time $t_{1/2}$ ± SD are indicated.

(**C**) FRAP analysis of Tem1 at dSPB in metaphase and anaphase. Cells of y3900 were grown and imaged at room temperature in SC medium + 2% glucose + 100 µM IAA.

(**D**) dSPB localization of Tem1 in cells with SPB-tethered GAP. Cells of y2015 (*BFA1*, n = 54 cells), y2098 (*bfa1Δ*, n = 64 cells), and y2990 (*SPC72-BFA1*, n = 48 cells) were grown at 25 °C in SC medium + 2% glucose and imaged every 3 minutes for 4 hours. Solid lines represent the average. Shaded areas represent 95% confidence intervals.

(**E**) Proposed model for GAP and Tem1 localization at the SPB. Under wildtype condition (low [Tem1^{GTP}] in the cell), only a fraction of the GAP complex at the dSPB is bound to Tem1^{GTP} in both metaphase and anaphase. While more GAP complex is recruited to dSPB in anaphase, the fraction of GAP bound to Tem1^{GTP} does not change between metaphase and anaphase. In cells with high [Tem1^{GTP}] such as with *TEM1Q79L*, most of the GAP complex are bound to [Tem1^{GTP}].

(**F**) dSPB localization of Tem1 (*WT* or *Q79L*) and Bfa1 (expressing *TEM1* or *TEM1Q79L*) in cells with Cdc15 depletion. Cells of y3900 (*TEM1*, n = 16 cells), y3903 (*TEM1Q79L*, n = 35 cells), y4123 (Bfa1 in *TEM1*, n = 24 cells), and y4122 (Bfa1 in *TEM1QL*, n = 32 cells) were grown at 25 °C in SC medium + 2% glucose + 100 μM IAA and imaged every 3 minutes for 4 hours. Solid lines represent the average. Shaded areas represent 95% confidence intervals.

Figure 6: SPB localization creates high local concentration of Tem1 for Cdc15 activation.

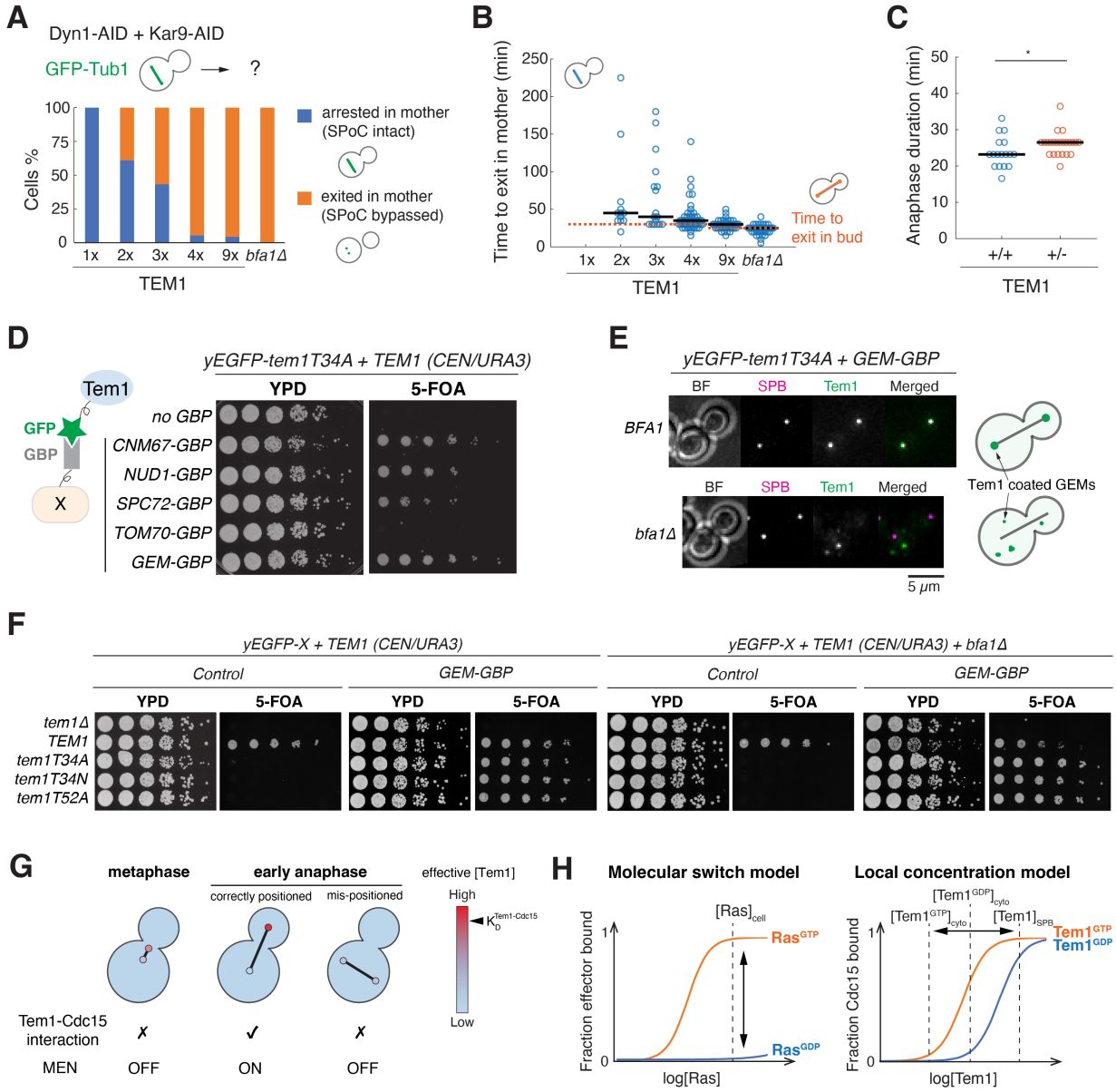

(**A-B**) Evaluation of the SPoC integrity in cells with different amount of Tem1. Cells of y3733 (1x*TEM1*, *n* = 102 cells), y3729 (2x*TEM1*, *n* = 72 cells), y3816 (3x*TEM1*, *n* = 64 cells), y3730 (4x*TEM1*, *n* = 102 cells), y3732 (9x*TEM1*, *n* = 101 cells), and y3815 (*bfa1Δ*, *n* = 65 cells) were grown at 25 °C in SC medium + 2% glucose + 100 μM IAA to induce spindle mispositioning by depleting Dyn1 and Kar9 and imaged every 5 minutes for 5 hours. Status of the spindle and cell cycle stages were monitored with GFP-Tub1. For time to exit in mother (mispositioned spindle disassembled in the mother cell) in B, solid lines represent the median, red dashed line indicate the median time to exit in bud (normal anaphase progression with correctly positioned spindle).

(**C**) Distribution of anaphase duration for diploid cells with two or one copy of *yEGFP-TEM1*. Cells of y3713 (+/+, n = 20 cells) and y3711 (+/-, n = 26 cells) were grown at 25°C in SC medium + 2% glucose and imaged every 3 minutes for 4 hours. Solid lines represent the median. *$p < 0.05$ by two-sided Wilcoxon rank sum test.

(**D**) Complementation analysis of *tem1T34A* with and without tethering to different GBP fusion proteins. 5-fold serial dilutions of strains y3203/y3305/y3500/y3499/y3501/y3502 were spotted onto plates with or without 5-FOA and incubated at 25°C for 2 to 3 days.

(**E**) Representative localization of GEM-tethered Tem1T34A in the presence or absence of *BFA1*. Cells of y3630 and y3557 were grown at 25 °C in SC medium + 2% glucose and imaged every 3 minutes for 4 hours.

(**F**) Complementation analysis of different Tem1 mutants tethered to GEMs in the presence or absence of *BFA1*. 5-fold serial dilutions of strains y2891/y3202/y3203/y3204/y3214, y3970/y3973/y3502/y3976/y3985, y3971/y3974/y3948/y3977/y3986, and y3972/y3975/y3945/y3978/y3987 were spotted onto plates with or without 5-FOA and incubated at 25°C for 2 to 3 days.

(**G**) Proposed model for Tem1 regulation.

(**H**) Comparison between the canonical molecular switch model and the concentration model for Tem1.

Figure S1: Biochemical characterization of Tem1.

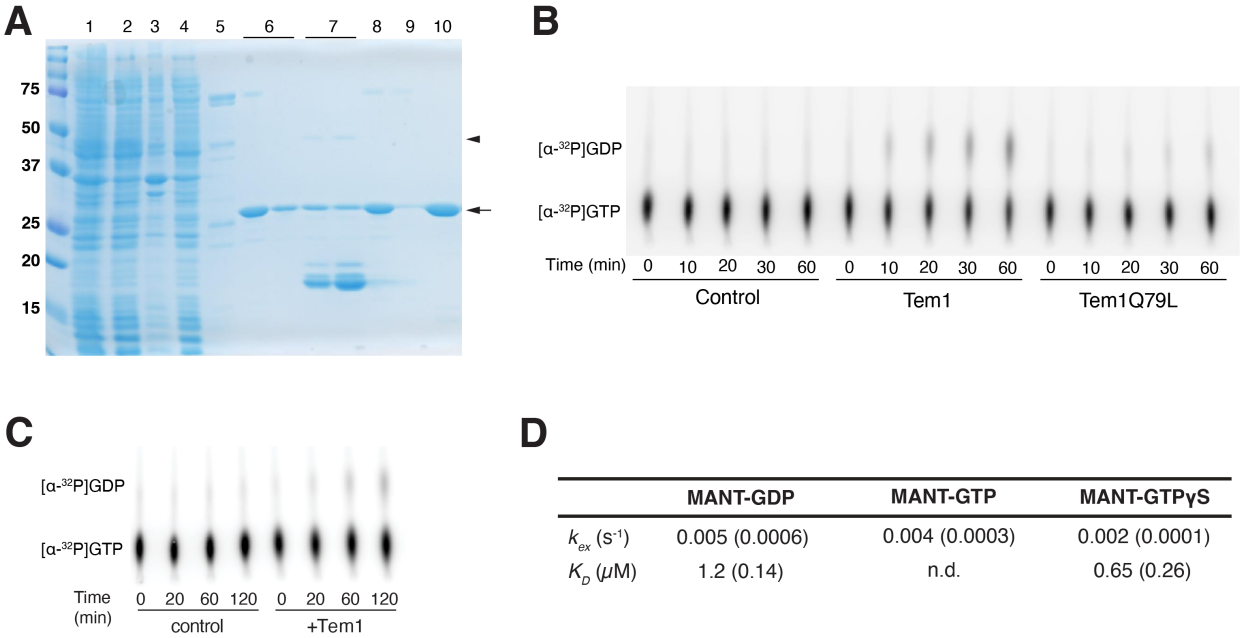

	MANT-GDP	MANT-GTP	MANT-GTPγS
k_{ex} (s^{-1})	0.005 (0.0006)	0.004 (0.0003)	0.002 (0.0001)
K_D (μM)	1.2 (0.14)	n.d.	0.65 (0.26)

(**A**) Purification of Tem1. Tem1 was expressed in *E. coli* as a 14xHis-SUMO-Tem1 fusion with p2579. *Lane 1*, lysate; *lane 2*, soluble fraction; *lane 3*, insoluble fraction; *lane 4*, flowthrough of Ni-NTA column; *lane 5*, wash with lysis buffer; *lane 6*, elution after overnight digest with SENP protease which contains cleaved Tem1; *lane 7*, elution with high imidazole buffer (250 mM imidazole) where the remaining 14xHis-SUMO and uncut fusion protein were eluted; *lane 8*, input for Mono S column; *lane 9*, wash with buffer A; *lane 10*, combined peak elution of Tem1 from Mono S. Arrowhead marks 14xHis-SUMO-Tem1 fusion (41 kDa) and arrow marks Tem1 (27 kDa).

(**B**) An example of raw thin layer chromatography (TLC) results for the GTPase activity of recombinantly purified Tem1 and the hydrolysis deficient mutant Tem1Q79L. No protein was added to the control sample (buffer only).

(**C**) An example of raw data for Fig. 1D.

(**D**) Summary of biochemical properties of Tem1 *in vitro*. Shown are the averages of three independent experiments and SD in parentheses. n.d., not determined (due to GTP hydrolysis). The difference of the observed exchange rate between MANT-GTP and MANT-GTPγS ($k_{obs} \approx k_{off}$ (GTP or GTPγS) + $k_{hydrolysis}$) is likely not driven by GTP hydrolysis as previously assumed in filter-binding assays because GTP hydrolysis occurs at a rate an order of magnitude slower than dissociation ($k_{obs} \sim 10^{-3}$ s^{-1}, while $k_{hydrolysis} \sim 10^{-4}$ s^{-1}). Rather, we think that the observed rates

reflect differences in affinity or off rate of the nucleotides ($k_{obs} \approx k_{off}$, when $k_{hydrolysis} << k_{obs}$). The higher affinity for MANT-GTPγS relative to MANT-GDP is consistent with the lower exchange rate for MANT-GTPγS we observed.

Figure S2: N-terminal fusion has a minimal perturbation on Tem1.

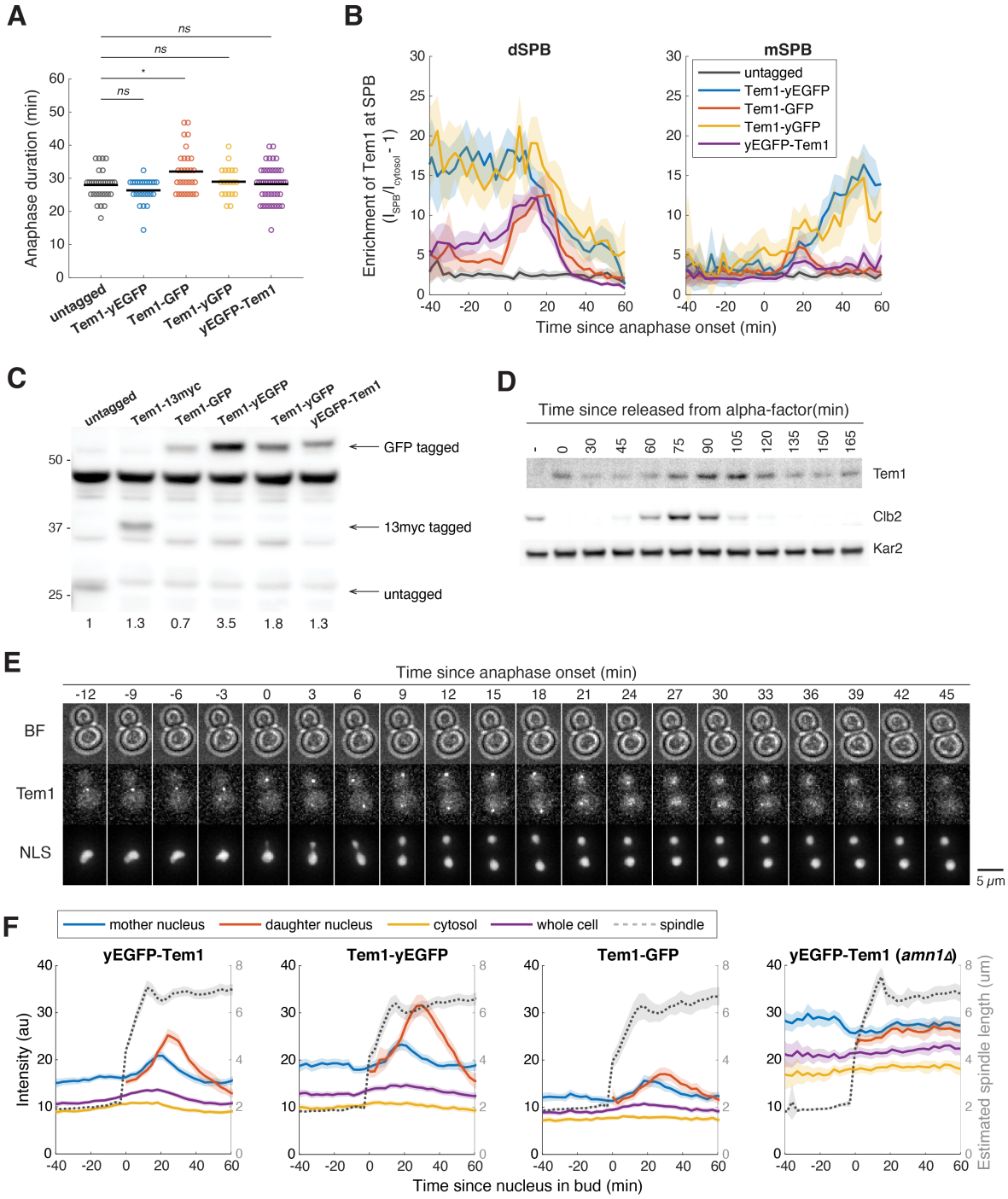

(**A-B**) Anaphase duration (A) and SPB localization (B) for different Tem1 fusions (y1008, y1267, y1271, y1739, and y1748; *n* = 39, 35, 39, 28, and 62 cells respectively) measured using the SPB marker Spc42-mScarlet-I. Cells were grown at 25 °C in SC medium + 2% glucose and imaged every 3 minutes for 4 hours. For (A), solid lines represent the median. *ns*, not significant

($p > 0.05$), *$p < 0.05$ by two-sided Wilcoxon rank sum test. For (B), solid lines represent the mean, shaded areas represent 95% confidence intervals. *TEM1-yEGFP* (codon-optimized eGFP) is known to be hyperactive (SPoC defective) whereas *TEM1-GFP* (not codon-optimized for yeast) is hypoactive as cells expressing Tem1-GFP delays exit from mitosis for more than 3 minutes. Tem1-yGFP (codon-optimized GFP) behaves more like Tem1-yEGFP rather than Tem1-GFP for SPB localization and anaphase length indicating it is the codon usage, likely due to changes in expression level as shown in (B), that is responsible for the difference in activity and localization profiles.

(**C**) Expression level of different Tem1 fusions. Whole-cell lysates of exponentially growing yA2587 (untagged), yA1828 (Tem1-13myc), yA22523 (Tem1-GFP), yA21089 (Tem1-yEGFP), y1724 (Tem1-yGFP), and y1735 (yEGFP-Tem1) were analyed by western blot with serum against Tem1. Cells were grown in YPD at 30 °C. C-terminal fusions of Tem1 stabilize the protein (unless a non-codon optimized GFP fusion is used). N-terminal fusion yEGFP-Tem1 is expressed at a level similar to wild-type Tem1 (1.3x) and cells expressing this fusion exit from mitosis at a rate similar to untagged cells (A).

(**D**) Tem1 level is cell cycle regulated. yA2587 (wild-type untagged strain) was arrested in G1 with α-factor (5 μg/ml) followed by release into YPD lacking pheromone. The amount of Tem1 protein were analyzed in whole-cell lysates by Western blot with anti-Tem1 serum. Clb2 was analyzed to determine when cells were in mitosis. Kar2 was used as internal loading control.

(**E**) Localization of Tem1 during the cell cycle where Tem1 is imported into the nucleus after exit from mitosis for degradation. y1879 (*yEGFP-TEM1* and NLS_{SV40}*-2xmCherry*) cells were grown at 25 °C in SC medium + 2% glucose and imaged every 3 minutes for 4 hours.

(**F**) Quantification of nuclear import and degradation for different Tem1 fusions. y1879 (yEGFP-Tem1, $n = 90$ cells), y1673 (Tem1-yEGFP, $n = 63$ cells), y1671 (Tem1-GFP, $n = 38$ cells), y3697 (*amn1Δ*, a control for no nuclear import/degradation, $n = 33$ cells) cells were grown at 25 °C in SC medium + 2% glucose and imaged every 3 minutes for 4 hours. Lines represent the average; shaded areas represent 95% confidence intervals. Albeit at different expression levels, all Tem1 fusions undergo Amn1 mediated nuclear import and degradation, ruling out a defect in this path of degradation.

Figure S3: Tethering Tem1 to the SPB rescues the lethality of nucleotide binding mutants of Tem1.

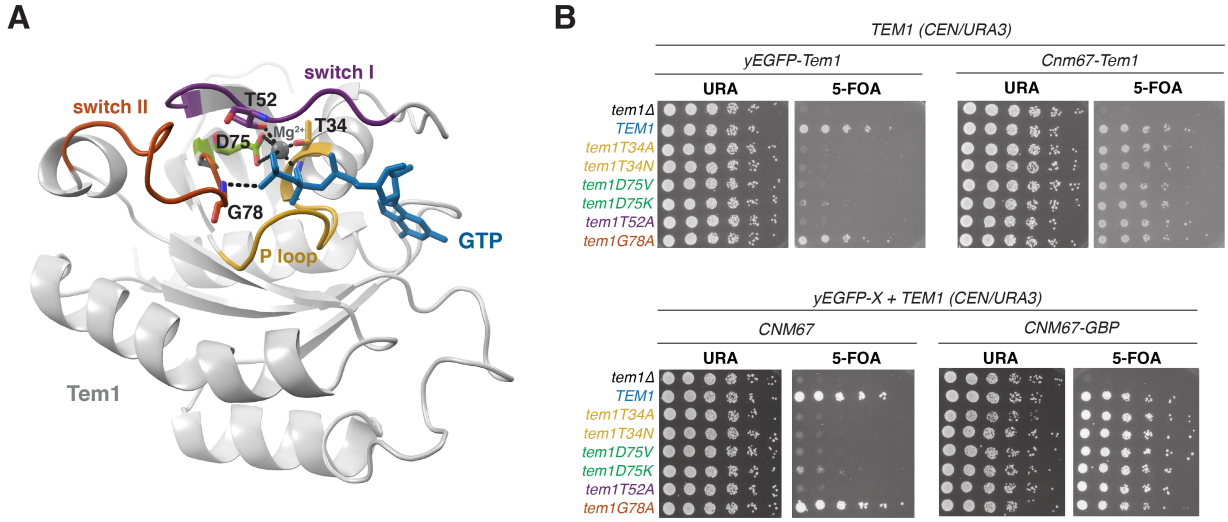

(**A**) Mutated residues in Tem1. A model of Tem1 (residues 13–187 containing the core GTPase domain) was downloaded from Swiss Model (P38987_20210204) using Rab35 (GTP)-RUSC2 as a template. Tem1 backbone (gray ribbon), GTP (cyan), Mg^{2+} (dark gray sphere), P-loop with T34 (yellow), switch-I with T52 (purple), switch-II with G78 (orange) and D75 (green). T34, T52, and D75 coordinate the Mg^{2+} atom while G78 forms hydrogen bond with the γ-phosphate (dashed lines). T34 (Ras-S17) and D75 (Ras-D57) contribute to nucleotide binding and mutations in these residues have been shown to bias affinity toward GDP over GTP for Ras. T52 (Ras-T35) and G78 (Ras-G60) are invariant residues in switch I/II regions of small GTPases that form key contacts with the γ-phosphate in GTP to stabilize the active confirmation that is used by regulatory proteins and effectors to 'sense' the nucleotide status of the small GTPases.
(**B**) Complementation analysis of Tem1 mutants with and without tethering to the SPB via direct fusion to Cnm67 (Cnm67-Tem1) or using yGFP-Tem1 + Cnm67-GBP combo. 5-fold serial dilutions of strains y2891/y3202/y3203/y3204/y3206/y3207/y3214/y3205 (untethered) and y2891/y2893/y2927/y3187/y3190/y3191/y3189/y3188 (direct fusion as Cnm67-Tem1) or y3303/y3304/y3305/y3306/y3308/y3309/y3310/y3307 (with *CNM67-GBP*) were spotted onto plates with or without 5'-fluoroorotic acid (5-FOA) and incubated at 25°C for 3 to 4 days. The presence of 5-FOA selects cells that are viable after losing the *TEM1 (URA3/CEN)* plasmid. Mutations in T34, D75, and T52 render Tem1 inactive and severely reduce viability. In contrast, the switch-II effector mutant Tem1G78A is active.

Figure S4: Localization of Tem1 to the SPB depends on the GAP complex Bub2-Bfa1.

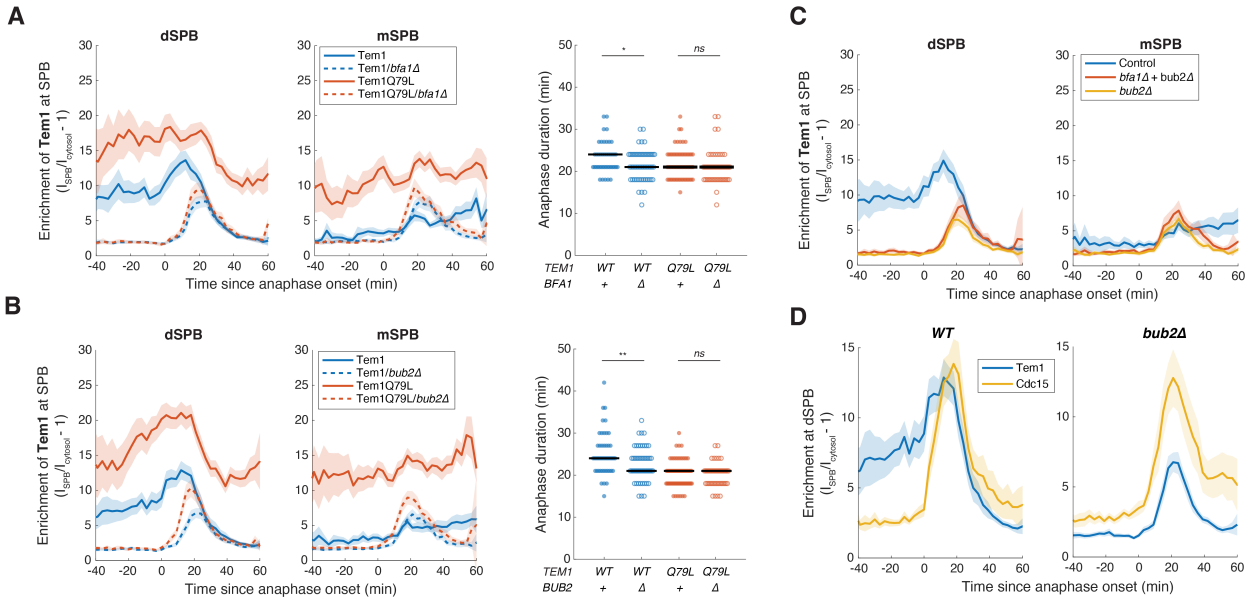

(**A**) SPB localization of Tem1 or the GTP-locked Tem1Q79L with or without the GAP component *BFA1* and the anaphase duration for the corresponding cells. Cells of y2015 (Tem1, n = 54 cells), y2098 (Tem1 in *bfa1Δ*, n = 64 cells), y2019 (Tem1Q79L, n = 79 cells), and y2133 (Tem1Q79L in *bfa1Δ*, n = 64 cells) were grown at 25 °C in SC medium + 2% glucose and imaged every 3 minutes for 4 hours. Solid lines represent the median. *ns*, not significant ($p > 0.05$), *$p < 0.05$ by two-sided Wilcoxon rank sum test.

(**B**) SPB localization of Tem1 or the GTP-locked Tem1Q79L with or without the GAP component *BUB2* and the anaphase duration for the corresponding cells. Cells of y1748 (Tem1, n = 65 cells), y1929 (Tem1 in *bub2Δ*, n = 72 cells), y1824 (Tem1Q79L, n = 91 cells), and y1930 (Tem1Q79L in *bub2Δ*, n = 64 cells) were grown at 25 °C in SC medium + 2% glucose and imaged every 3 minutes for 4 hours. For SPB localization, solid lines represent the average. Shaded areas represent 95% confidence intervals. For anaphase duration, solid lines represent the median. *ns*, not significant ($p > 0.05$), **$p < 0.01$ by two-sided Wilcoxon rank sum test.

(**C**) SPB localization of Tem1 with or without *BFA1* & *BUB2*. Cells of y2015 (Tem1, n = 44 cells), y3717 (Tem1 in *bfa1Δ*+*bub2Δ*, n = 42 cells), and y3718 (Tem1 in *bub2Δ*, n = 50 cells) were grown at 25 °C in SC medium + 2% glucose and imaged every 3 minutes for 4 hours. Solid lines represent the average. Shaded areas represent 95% confidence intervals.

(**D**) Comparison of SPB localization for Tem1 and Cdc15 in the presence or absence of *BUB2*. Same data as in Fig. 3A.

Figure S5: Localization of Tem1 to the SPB depends on Cdc15.

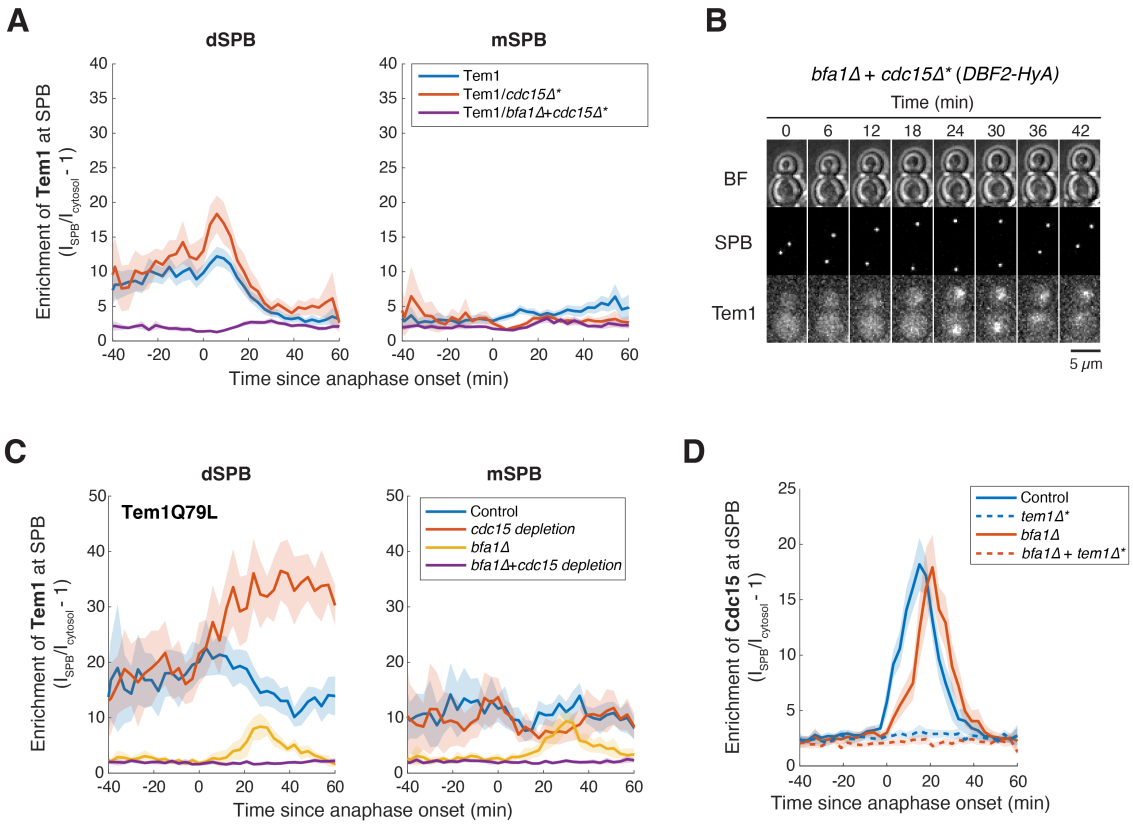

(**A**) SPB localization of Tem1 or Tem1Q79L with or without *BFA1&CDC15*. Cells of y2898 (Tem1, *n* = 61 cells), y2910 (Tem1 in *cdc15Δ*, *n* = 24 cells), and y2899 (Tem1 in *bfa1Δ+cdc15Δ*, *n* = 42 cells) were grown at 25 °C in SC medium + 2% glucose and imaged every 3 minutes for 4 hours. * denotes the presence of the hyperactive *DBF2-HyA* which rescues *cdc15Δ*.

(**B**) Representative localization of Tem1 in *bfa1Δ+cdc15Δ* cell kept alive with *DBF2-HyA* (y2899). No SPB localization was observed but nuclear import and degradation still occurs (which contributes to the slight increase in SPB enrichment in late anaphase as shown in A).

(**C**) SPB localization of Tem1Q79L with or without depleting Cdc15 (*cdc15-AID* +/- *osTIR*) in the presence or absence of *BFA1*. Cells of y3231 (Tem1Q79L control, *n* = 18 cells), y3226 (Tem1Q79L with Cdc15 depletion, *n* = 14 cells), y3230 (Tem1Q79L in *bfa1Δ*, *n* = 16 cells), and y3225 (Tem1Q79L in *bfa1Δ* with Cdc15 depletion, *n* = 17 cells) were grown at 25 °C in SC medium + 2% glucose + 200 μM auxin IAA and imaged every 3 minutes for 4 hours.

(**D**) SPB localization of Cdc15 still depends on Tem1 in the absence of the GAP. Cells of y1275 (Cdc15-yEGFP, *n* = 75 cells), y2945 (Cdc15-yEGFP in *tem1Δ*, *n* = 41 cells), y2958 (Cdc15-yEGFP in *bfa1Δ*, *n* = 37 cells), and y3010 (Cdc15-yEGFP in *tem1Δ*+*bfa1Δ*, *n* = 37 cells) were grown at 25 °C in SC medium + 2% glucose and imaged every 3 minutes for 4 hours. Cells with *tem1Δ* were kept alive with *DBF2-HyA*.

Figure S6: Interaction between Tem1 and Cdc15 or the GAP complex.

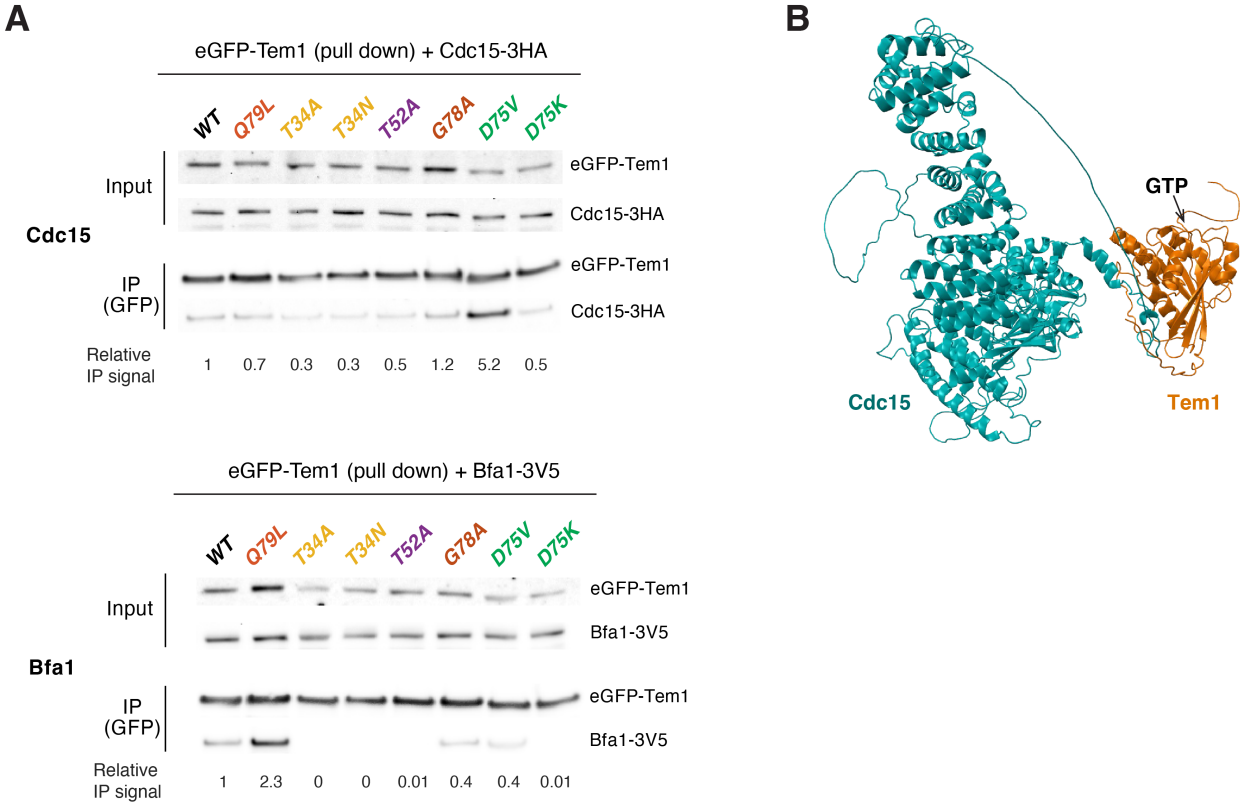

(**A**) Interaction between different Tem1 mutants and Cdc15 or the GAP complex via co-immunoprecipitation. yEGFP-Tem1 was immunoprecipitated from exponentially grown cells of y2885/y2886/y3209/y3210/y3208/y3211/y3212/y3213 or y3452/y3472/y3457/y3458/y3456/y3455/y3459/y3460 and the presence of Cdc15-3HA or Bfa1-3V5 were analyzed by Western blot analysis.

(**B**) AlphaFold2 predicted structure of Tem1-Cdc15 complex.

Figure S7: GAP stimulated GTP hydrolysis drives the fast turnover of Tem1 at the dSPB.

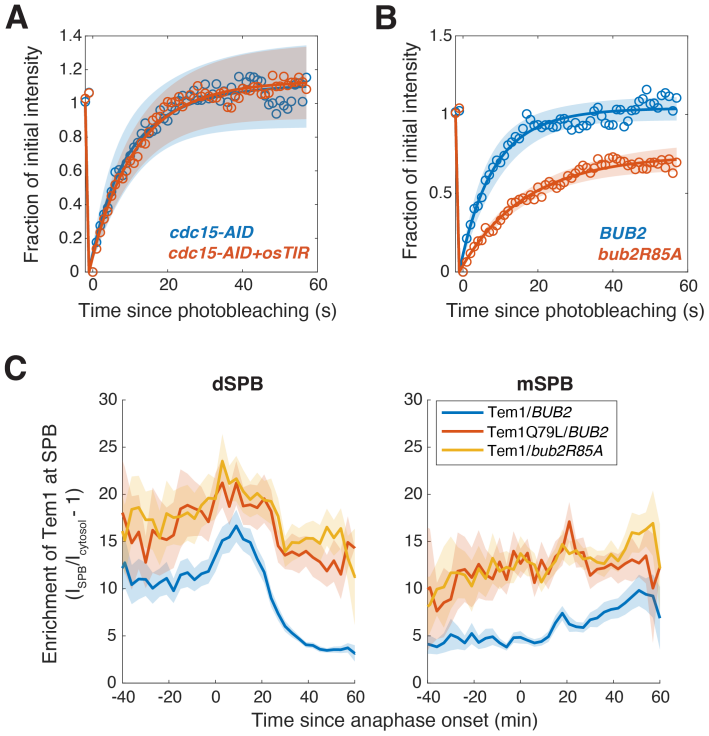

(**A**) FRAP analysis of Tem1 at dSPB in anaphase with or without depleting Cdc15. Cells of y3901 (*cdc15-AID*, *n* = 6 cells) and y3900 (*cdc15-AID+OsTIR*, *n* = 9 cells) were grown and imaged at room temperature in SC medium + 2% glucose + 100 µM IAA. Circles represent the average measurements of double normalized fluorescence intensities after correcting for photo-bleaching during acquisition. Solid lines are the average fit and shaded areas represent SD.

(**B**) FRAP analysis of Tem1 at dSPB in anaphase with hydrolysis defective Bub2 mutant (*bub2R85A*). Cells of y2015 (*BUB2*, *n* = 6 cells) and y2971 (*bub2R85A*, *n* = 6 cells) were grown and imaged at room temperature in SC medium + 2% glucose. Circles represent the average measurements of double normalized fluorescence intensities after correcting for photo-bleaching during acquisition. Solid lines are the average fit and shaded areas represent SD.

(**C**) SPB localization of Tem1 in cells with defective GTP hydrolysis. Cells of y2015 (*WT*, *n* = 69 cells), y2019 (*TEM1Q79L*, *n* = 42 cells), and y2971 (*bub2R85A*, *n* = 51 cells) were grown at 25 °C in SC medium + 2% glucose and imaged every 3 minutes for 4 hours. Solid lines represent the average. Shaded areas represent 95% confidence intervals.

Figure S8: A simple model for Tem1's nucleotide cycle.

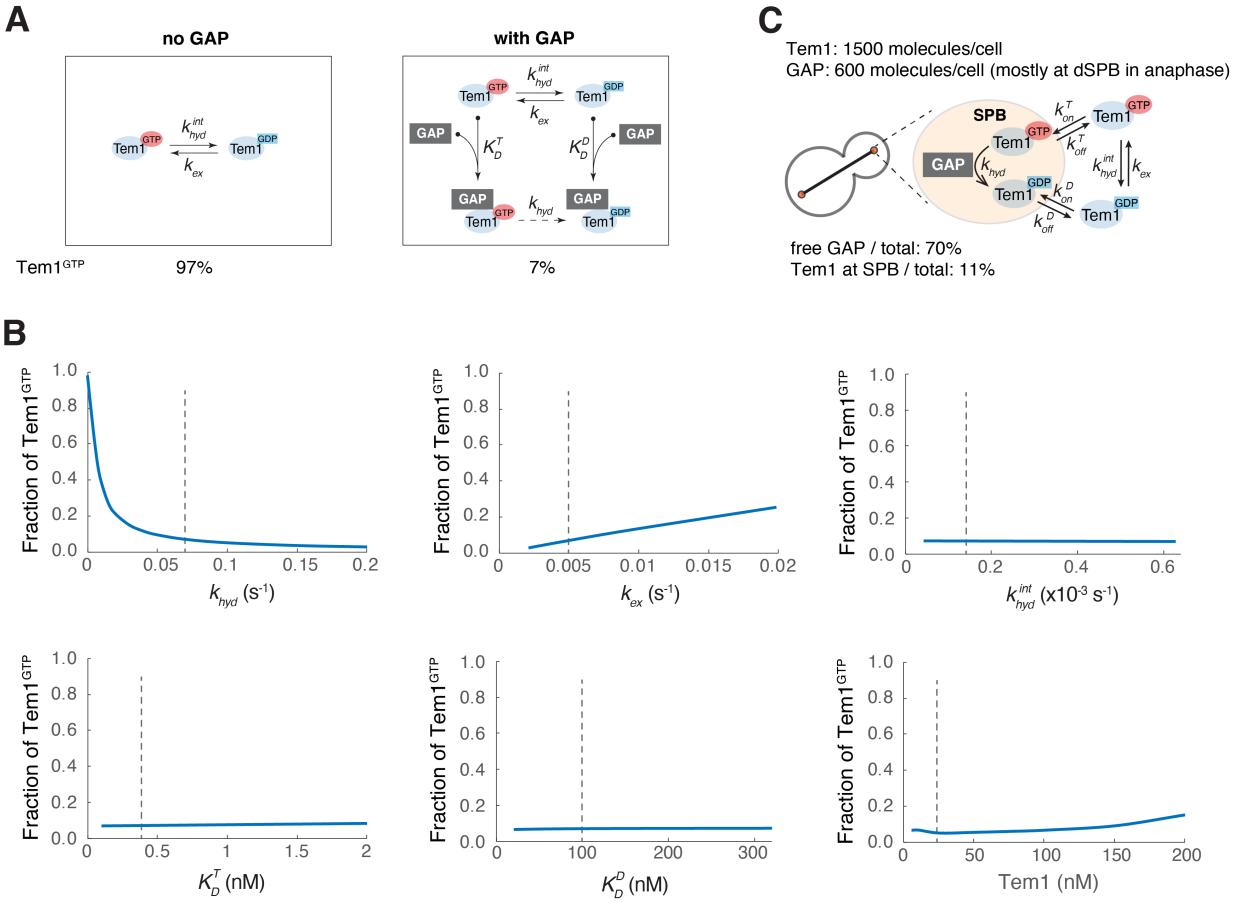

(**A**) A simplified model for Tem1's GTP/GDP cycle with or without the GAP.

(**B**) Fraction of Tem1^{GTP} as predicted by the model (with GAP) as a function of the GAP-stimulated GTP hydrolysis rate k_{hyd}, Tem1's intrinsic nucleotide exchange rate k_{ex}, Tem1's intrinsic GTP hydrolysis rate k_{hyd}^{int}, dissociation constant for GAP binding Tem1^{GTP} K_D^T, dissociation constant for GAP binding Tem1^{GDP} K_D^D, or Tem1 concentration in the cell. Dashed lines represent the values used to make the predictions shown in A.

(**C**) A simplified model for Tem1's GTP/GDP cycle at dSPB in anaphase. The same model parameters were used as in A.

Figure S9: SPB-tethered Bfa1 retains GAP activity.

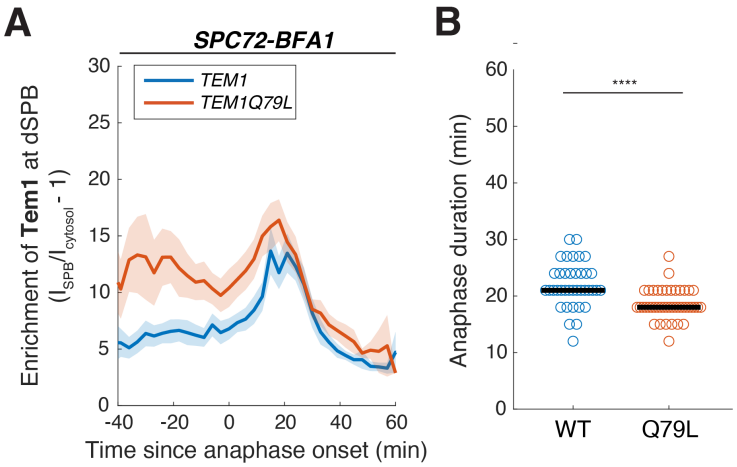

(**A**) SPB localization of Tem1 and Tem1Q79L in cells with SPB-tethered Bfa1 (*SPC72-BFA1*). Cells of y2990 (Tem1, n = 48 cells) and y2991 (Tem1Q79L, n = 54 cells) were grown at 25 °C in SC medium + 2% glucose and imaged every 3 minutes for 4 hours. Solid lines represent the average. Shaded areas represent 95% confidence intervals.

(**B**) Distribution of anaphase duration for cells expressing *TEM1* or *TEM1Q79L* in combination with *SPC72-BFA1*. Same cells as in (A). Solid lines represent the median. ****$p < 0.0001$ by two-sided Wilcoxon rank sum test.

Figure S10: MEN activity is sensitive to Tem1 level.

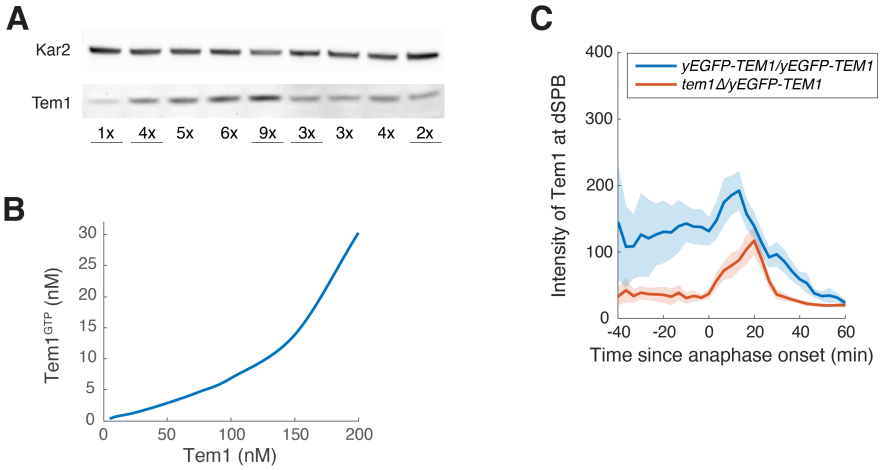

(**A**) Quantification of Tem1 expression level. Whole-cell lysates of exponentially growing cells with different copy numbers of Tem1 integrated at the *leu2* locus. Relative expression of Tem1 (indicated below) was quantified and normalized to the signal of Kar2. Underscored lanes represent strains used in this study: yA2587 (1xTem1, WT), y3693 (4xTem1), y3696 (9xTem1), y3692 (3xTem1), y3691 (2xTem1).

(**B**) Predicted $Tem1^{GTP}$ concentration as a function of Tem1 concentration in the cell (using the model illustrated in Fig. S8).

(**C**) SPB localization of Tem1 in diploid cells with two or one copy of *yEGFP-TEM1*. Cells of y3713 (two copies, n = 20 cells) and y3711 (one copy, n = 26 cells) were grown at 25°C in SC medium + 2% glucose and imaged every 3 minutes for 4 hours. Solid lines represent the average. Shaded areas represent 95% confidence intervals. Note that the SPB localization profile of Tem1 heterozygous deletion (~50% expression level) resembles the hypomorphic Tem1-GFP (Fig. S2, ~ 70% WT level).

Figure S11: Concentrating Tem1 by tethering to GEMs activates the MEN.

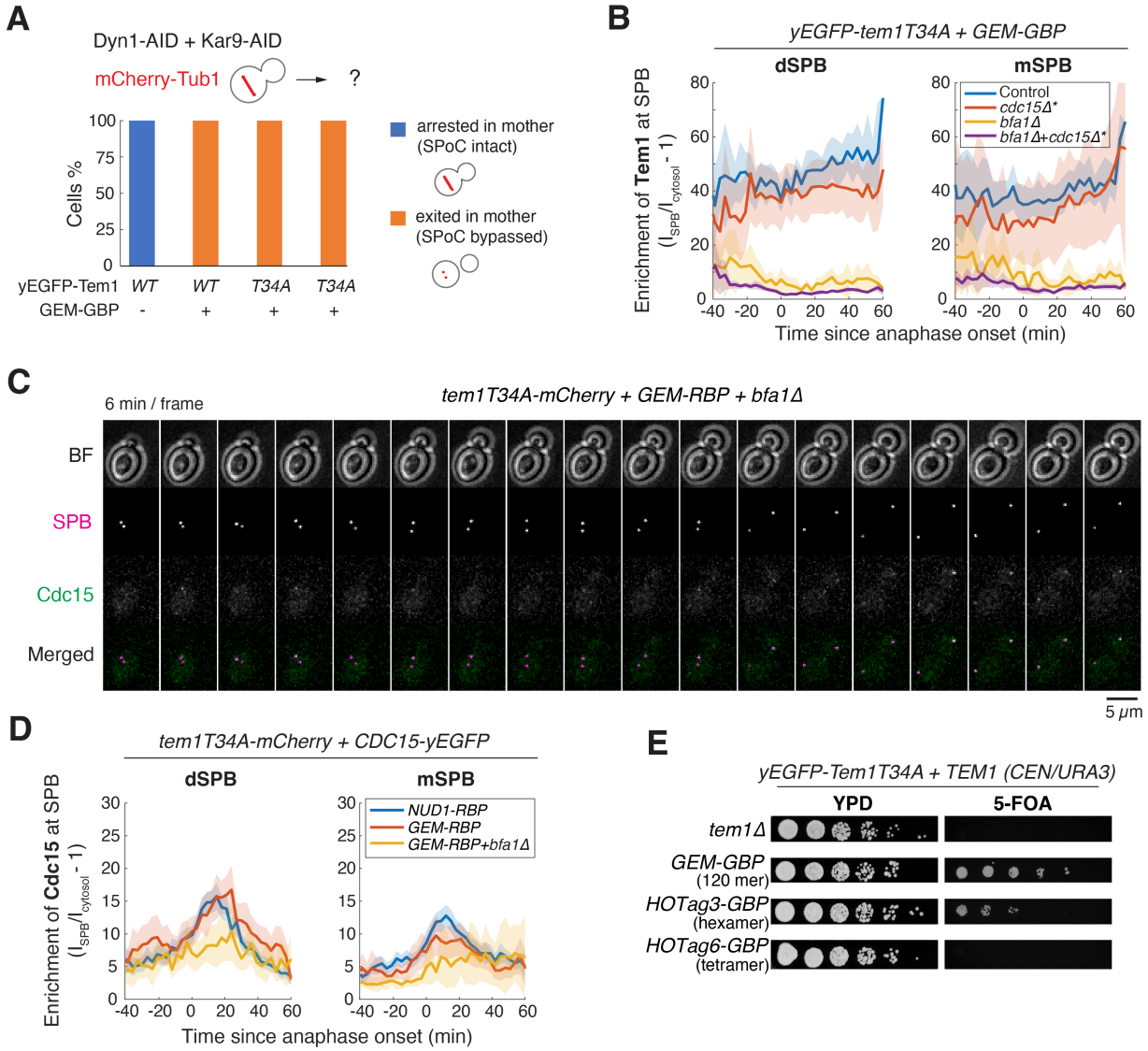

(**A**) Evaluation of the SPoC integrity in cells with Tem1 tethered to GEMs. Cells of y4097 (yEGFP-*TEM1*, *n* = 31 cells), y4095 (yEGFP-*TEM1* + GEM-GBP, *n* = 40 cells), y4100 (yEGFP-*tem1T34A* + GEM-GBP, *n* = 40 cells) and y4101 (yEGFP-*tem1T34A* + GEM-GBP, *n* = 36 cells), were grown at 25 °C in SC medium + 2% glucose + 100 μM IAA to induce spindle mispositioning by depleting Dyn1 and Kar9 and imaged every 5 minutes for 5 hours. Status of the spindle and cell cycle stages were monitored with mCherry-Tub1.

(**B**) SPB localization of GEM-tethered Tem1T34A in cells with or without *BFA1* or *CDC15*. Cells of y3630 (*BFA1*+*CDC15*, *n* = 27 cells), y3631 (*BFA1*+*cdc15Δ*, *n* = 18 cells), y3557 (*bfa1Δ*+*CDC15*, *n* = 21 cells), and y3510 (*bfa1Δ*+*cdc15Δ*, *n* = 21 cells) were grown at 25°C in

SC medium + 2% glucose and imaged every 3 minutes for 4 hours. Solid lines represent the average. Shaded areas represent 95% confidence intervals.

(**C-D**) SPB localization of Cdc15 in cells with SPB- or GEM-tethered Tem1T34A. Cells of y3585 (*NUD1-RBP*, *n* = 67 cells), y3589 (*GEM-RBP*, *n* = 35 cells), and y3588 (GEM-RBP+*bfa1Δ*, *n* = 14 cells) were grown at 25°C in SC medium + 2% glucose and imaged every 3 minutes for 4 hours. Solid lines represent the average. Shaded areas represent 95% confidence intervals.

Representative localization of Cdc15 in y3588 is shown in C and quantification of anaphase duration as well as max enrichment of Cdc15 are shown in D.

(**E**) Complementation analysis of *tem1T34A* with and without tethering to different GBP fusion proteins. 5-fold serial dilutions of strains y3970/y3502/y3956/y3958 were spotted onto plates with or without 5-FOA and incubated at 25°C for 2 to 3 days.

Table S1. Yeast strains used in this study.

Strain	Relevant Genotype
A2587	*MATa, ade2-1, leu2-3, ura3, trp1-1, his3-11,15, can1-100, GAL, psi+ (wild-type W303)*
A1828	*MATa, TEM1-13Myc*
A21089	*MATa, TEM1-yEGFP::SpHIS5*
A22523	*MATa, TEM1-GFP:HisMx6*
y1008	*MATa, SPC42-mScarlet-I::LEU2*
y1267	*MATa, SPC42-mScarlet-I::LEU2, TEM1-yEGFP::SpHIS5*
y1271	*MATa, SPC42-mScarlet-I::LEU2, TEM1-GFP:HisMx6*
y1275	*MATa, SPC42-mScarlet-I::LEU2, CDC15-yEGFP::KanMX6*
y1374	*MATa, SPC42-mScarlet-I::LEU2, BFA1-yEGFP::KanMX6*
y1378	*MATa, SPC42-mScarlet-I::LEU2, BUB2-yEGFP::KanMX6*
y1671	*MATa, TEM1-GFP:HisMx6, ura3:pRS306-pCTS1-2xmCherry-SV40NLS:URA3*
y1673	*MATa, TEM1-yEGFP::SpHIS5, ura3:pRS306-pCTS1-2xmCherry-SV40NLS:URA3*
y1693	*MATa, SPC42-mScarlet-I::LEU2, CDC15-yEGFP::KanMX6, bub2::HIS3*
y1724	*MATa, TEM1-yGFP(S65T)::SpHIS5*
y1735	*MATa, yEGFP-TEM1*
y1739	*MATa, SPC42-mScarlet-I::LEU2, TEM1-yGFP(S65T)::SpHIS5*
y1748	*MATa, SPC42-mScarlet-I::LEU2, yEGFP-TEM1*
y1824	*MATa, SPC42-mScarlet-I::LEU2, yEGFP-TEM1(Q79L)*
y1879	*MATa, yEGFP-TEM1, ura3:pRS306-pCTS1-2xmCherry-SV40NLS:URA3*
y1929	*MATa, SPC42-mScarlet-I::LEU2, yEGFP-TEM1, bub2::HIS3*
y1930	*MATa, SPC42-mScarlet-I::LEU2, yEGFP-TEM1(Q79L), bub2::HIS3*
y2015	*MATa, SPC42-mScarlet-I::LEU2, yEGFP-TEM1::KanMX6*
y2019	*MATa, SPC42-mScarlet-I::LEU2, yEGFP-TEM1(Q79L)::KanMX6*
y2098	*MATa, SPC42-mScarlet-I::LEU2, yEGFP-TEM1::KanMX6, bfa1::HIS3*
y2133	*MATa, SPC42-mScarlet-I::LEU2, yEGFP-TEM1(Q79L)::KanMX6, bfa1::HIS3*
y2194	*MATa, SPC42-mScarlet-I::LEU2, BFA1-yEGFP::KanMX6, TEM1Q79L::hphNT1*
y2761	*MATa, CDC15-3HA::His3MX*
y2885	*MATa, CDC15-3HA::His3MX, yEGFP-TEM1::KanMX6*
y2886	*MATa, CDC15-3HA::His3MX, yEGFP-TEM1(Q79L)::KanMX6*
y2891	*MATa, tem1::KanMx6, pRS316-yEGFP-TEM1*
y2892	*MATalpha, tem1::KanMx6, pRS316-yEGFP-TEM1*
y2893	*MATa, pRS316-yEGFP-TEM1*
y2898	*MATa, SPC42-mScarlet-I::LEU2, yEGFP-TEM1::KanMX6, DBF2-HyA::hphNT1*
y2899	*MATa, SPC42-mScarlet-I::LEU2, yEGFP-TEM1::KanMX6, DBF2-HyA::hphNT1, bfa1::HIS3, cdc15::HIS3*
y2927	*MATa, tem1::CNM67-tem1(T34A), pRS316-yEGFP-TEM1*
y2945	*MATa, cdc15::HIS3, leu2::CDC15-yEGFP::LEU2, SPC42-mScarlet-I::LEU2, pRS315-DBF2-HyA, tem1::KanMx6*
y2958	*MATa, SPC42-mScarlet-I::LEU2, CDC15-yEGFP::KanMX6, bfa1::HIS3*
y2971	*MATa, SPC42-mScarlet-I::LEU2, yEGFP-TEM1::KanMX6, bub2(R85A)*
y2990	*MATalpha, SPC42-mScarlet-I::LEU2, yEGFP-TEM1::KanMX6, SPC72-BFA1::LEU2, bfa1::TRP1*

y2991	*MATa, SPC42-mScarlet-I::LEU2, yEGFP-TEM1(Q79L)::KanMX6, SPC72-BFA1::LEU2, bfa1::TRP1*
y3010	*MATa, SPC42-mScarlet-I::LEU2, CDC15-yEGFP::KanMX6, pRS315-DBF2-HyA, tem1::KanMx6, bfa1::HIS3*
y3059	*MATa, yEGFP-Tem1::KanMX6, dbf2::DBF2-HyA::hphNT1*
y3099	*MATa, SPC42-mScarlet-I::LEU2, BFA1-yEGFP::KanMX6, bub2::HIS3*
y3147	*MATa, SPC42-mScarlet-I::LEU2, yEGFP-tem1(T52A)::KanMX6, DBF2-HyA::hphNT1*
y3167	*MATa, SPC42-mScarlet-I::LEU2, yEGFP-tem1(T34A)::KanMX6, DBF2-HyA::hphNT1*
y3171	*MATalpha, SPC42-mScarlet-I::LEU2, yEGFP-tem1(T34N)::KanMX6, DBF2-HyA::hphNT1*
y3187	*MATa, tem1::CNM67-tem1(T34N), pRS316-yEGFP-TEM1*
y3188	*MATa, tem1::CNM67-TEM1(G78A), pRS316-yEGFP-TEM1*
y3189	*MATa, tem1::CNM67-tem1(T52A), pRS316-yEGFP-TEM1*
y3190	*MATa, tem1::CNM67-tem1(D75V), pRS316-yEGFP-TEM1*
y3191	*MATa, tem1::CNM67-tem1(D75K), pRS316-yEGFP-TEM1*
y3202	*MATa, yEGFP-TEM1::KanMX6, pRS316-yEGFP-TEM1*
y3203	*MATa, yEGFP-tem1(T34A)::KanMX6, pRS316-yEGFP-TEM1*
y3204	*MATa, yEGFP-tem1(T34N)::KanMX6, pRS316-yEGFP-TEM1*
y3205	*MATa, yEGFP-TEM1(G78A)::KanMX6, pRS316-yEGFP-TEM1*
y3206	*MATa, yEGFP-tem1(D75V)::KanMX6, pRS316-yEGFP-TEM1*
y3207	*MATa, yEGFP-tem1(D75K)::KanMX6, pRS316-yEGFP-TEM1*
y3208	*MATa, CDC15-3HA::His3MX, yEGFP-tem1(T52A)::KanMX6, DBF2-HyA::hphNT1*
y3209	*MATa, CDC15-3HA::His3MX, yEGFP-tem1(T34A)::KanMX6, DBF2-HyA::hphNT1*
y3210	*MATa, CDC15-3HA::His3MX, yEGFP-tem1(T34N)::KanMX6, DBF2-HyA::hphNT1*
y3211	*MATa, CDC15-3HA::His3MX, yEGFP-TEM1(G78A)::KanMX6, DBF2-HyA::hphNT1*
y3212	*MATa, CDC15-3HA::His3MX, yEGFP-tem1(D75V)::KanMX6, DBF2-HyA::hphNT1*
y3213	*MATa, CDC15-3HA::His3MX, yEGFP-tem1(D75K)::KanMX6, DBF2-HyA::hphNT1*
y3214	*MATa, yEGFP-tem1(T52A)::KanMX6, pRS316-yEGFP-TEM1*
y3223	*MATalpha, SPC42-mScarlet-I::LEU2, yEGFP-TEM1::KanMX6, bfa1::HIS3, CDC15-AID*-9myc::hphNT1, leu2::pTEF1-osTIR::LEU2*
y3224	*MATalpha, SPC42-mScarlet-I::LEU2, yEGFP-TEM1::KanMX6, CDC15-AID*-9myc::hphNT1, leu2::pTEF1-osTIR::LEU2*
y3225	*MATa, SPC42-mScarlet-I::LEU2, yEGFP-TEM1(Q79L)::KanMX6, bfa1::HIS3, CDC15-AID*-9myc::hphNT1, leu2::pTEF1-osTIR::LEU2*
y3226	*MATalpha, SPC42-mScarlet-I::LEU2, yEGFP-TEM1(Q79L)::KanMX6, CDC15-AID*-9myc::hphNT1, leu2::pTEF1-osTIR::LEU2*
y3228	*MATa, SPC42-mScarlet-I::LEU2, yEGFP-TEM1::KanMX6, bfa1::HIS3, CDC15-AID*-9myc::hphNT1*
y3229	*MATa, SPC42-mScarlet-I::LEU2, yEGFP-TEM1::KanMX6, CDC15-AID*-9myc::hphNT1*
y3230	*MATa, SPC42-mScarlet-I::LEU2, yEGFP-TEM1(Q79L)::KanMX6, bfa1::HIS3, CDC15-AID*-9myc::hphNT1*
y3231	*MATa, SPC42-mScarlet-I::LEU2, yEGFP-TEM1(Q79L)::KanMX6, CDC15-AID*-9myc::hphNT1*
y3287	*MATa, yEGFP-TEM1(Q79L)::KanMX6, CNM67-GBP::His3MX6*
y3289	*MATa, yEGFP-TEM1::KanMX6, CNM67-GBP::His3MX6*
y3291	*MATa, yEGFP-tem1(T34A)::KanMX6, CNM67-GBP::His3MX6*
y3303	*MATa, tem1::KanMx6, pRS316-yEGFP-TEM1, CNM67-GBP::His3MX6*

y3304	*MATa, yEGFP-TEM1::KanMX6, pRS316-yEGFP-TEM1, CNM67-GBP::His3MX6*
y3305	*MATa, yEGFP-tem1(T34A)::KanMX6, pRS316-yEGFP-TEM1, CNM67-GBP::His3MX6*
y3306	*MATa, yEGFP-tem1(T34N)::KanMX6, pRS316-yEGFP-TEM1, CNM67-GBP::His3MX6*
y3307	*MATa, yEGFP-TEM1(G78A)::KanMX6, pRS316-yEGFP-TEM1, CNM67-GBP::His3MX6*
y3308	*MATa, yEGFP-tem1(D75V)::KanMX6, pRS316-yEGFP-TEM1, CNM67-GBP::His3MX6*
y3309	*MATa, yEGFP-tem1(D75K)::KanMX6, pRS316-yEGFP-TEM1, CNM67-GBP::His3MX6*
y3310	*MATa, yEGFP-tem1(T52A)::KanMX6, pRS316-yEGFP-TEM1, CNM67-GBP::His3MX6*
y3452	*MATa, yEGFP-TEM1::KanMX6, BFA1-3V5::HIS3*
y3455	*MATa, yEGFP-TEM1(G78A)::KanMX6, BFA1-3V5::HIS3*
y3456	*MATa, yEGFP-tem1(T52A)::KanMX6, DBF2-HyA::hphNT1, BFA1-3V5::HIS3*
y3457	*MATa, yEGFP-tem1(T34A)::KanMX6, DBF2-HyA::hphNT1, BFA1-3V5::HIS3*
y3458	*MATa, yEGFP-tem1(T34N)::KanMX6, DBF2-HyA::hphNT1, BFA1-3V5::HIS3*
y3459	*MATa, yEGFP-tem1(D75V)::KanMX6, DBF2-HyA::hphNT1, BFA1-3V5::HIS3*
y3460	*MATa, yEGFP-tem1(D75K)::KanMX6, DBF2-HyA::hphNT1, BFA1-3V5::HIS3*
y3461	*MATa, BFA1-3V5::HIS3*
y3472	*MATa, yEGFP-TEM1(Q79L)::KanMX6, BFA1-3V5::HIS3*
y3499	*MATa, yEGFP-tem1(T34A)::KanMX6, pRS316-yEGFP-TEM1, SPC72-GBP::His3MX6*
y3500	*MATa, yEGFP-tem1(T34A)::KanMX6, pRS316-yEGFP-TEM1, NUD1-GBP::His3MX6*
y3501	*MATa, yEGFP-tem1(T34A)::KanMX6, pRS316-yEGFP-TEM1, TOM70-GBP::His3MX6*
y3502	*MATa, yEGFP-tem1(T34A)::KanMX6, pRS316-yEGFP-TEM1, leu2::pRS305-pINO4-PfV-GS-GBP::LEU2*
y3510	*MATa, yEGFP-tem1(T34A)::KanMX6, leu2::pRS305-pINO4-PfV-GS-GBP::LEU2, cdc15::HIS3, DBF2-HyA::hphNT1, SPC42-mScarlet-I::LEU2, bfa1::TRP1*
y3557	*MATa, yEGFP-tem1(T34A)::KanMX6, leu2::pRS305-pINO4-PfV-GS-GBP::LEU2, SPC42-mScarlet-I::LEU2, bfa1::TRP1*
y3585	*MATa, SPC42-mScarlet-I::LEU2, CDC15-yEGFP::KanMX6, tem1T34A-mCherry-PIF6::NatMx6, NUD1-RBP::His3MX6*
y3588	*MATa, SPC42-mScarlet-I::LEU2, CDC15-yEGFP::KanMX6, tem1T34A-mCherry-PIF6::NatMx6, leu2::pRS305-pINO4-PfV-GS-RBP::LEU2, bfa1::HIS3*
y3589	*MATa, SPC42-mScarlet-I::LEU2, CDC15-yEGFP::KanMX6, tem1T34A-mCherry-PIF6::NatMx6, leu2::pRS305-pINO4-PfV-GS-RBP::LEU2*
y3630	*MATa, yEGFP-tem1(T34A)::KanMX6, leu2::pRS305-pINO4-PfV-GS-GBP::LEU2, SPC42-mScarlet-I::LEU2*
y3631	*MATa, yEGFP-tem1(T34A)::KanMX6, leu2::pRS305-pINO4-PfV-GS-GBP::LEU2, cdc15::HIS3, DBF2-HyA::hphNT1, SPC42-mScarlet-I::LEU2*
y3632	*MATa, SPC42-mScarlet-I::LEU2, BUB2-yEGFP::KanMX6, bfa1::HIS3*
y3691	*MATa, leu2:: YIplac128-TEM1::LEU2*
y3692	*MATa, leu2::2xYIplac128-TEM1::LEU2*
y3693	*MATa, leu2::3xYIplac128-TEM1::LEU2*
y3696	*MATa, leu2::8xYIplac128-TEM1::LEU2*
y3697	*MATa, ura3:pRS306-pCTS1-2xmCherry-SV40NLS:URA3, yEGFP-TEM1::KanMX6, amn1::natMX6*
y3711	*MATa/alpha, SPC42-mScarlet-I::LEU2/SPC42-mScarlet-I::LEU2, tem1::KanMx/yEGFP-TEM1::KanMx6*
y3713	*MATa/alpha, SPC42-mScarlet-I::LEU2/SPC42-mScarlet-I::LEU2, yEGFP-TEM1::KanMx/yEGFP-TEM1::KanMx6*
y3717	*MATa, SPC42-mScarlet-I::LEU2, yEGFP-TEM1::KanMX6, bub2::HIS3, bfa1::TRP1*

y3718	*MATa, SPC42-mScarlet-I::LEU2, yEGFP-TEM1::KanMX6, bub2::HIS3*
y3729	*MATa, DYN1-3V5-AID:KanMX6, KAR9-AID*-6HA:hphNT1, ura3::pTUB1-GFP-TUB1::URA3, his3::pTEF1-osTIR::HIS3, leu2::YIplac128-TEM1::LEU2*
y3730	*MATa, DYN1-3V5-AID:KanMX6, KAR9-AID*-6HA:hphNT1, ura3::pTUB1-GFP-TUB1::URA3, his3::pTEF1-osTIR::HIS3, leu2::3xYIplac128-TEM1::LEU2*
y3732	*MATa, DYN1-3V5-AID:KanMX6, KAR9-AID*-6HA:hphNT1, ura3::pTUB1-GFP-TUB1::URA3, his3::pTEF1-osTIR::HIS3, leu2::8xYIplac128-TEM1::LEU2*
y3733	*MATa, DYN1-3V5-AID:KanMX6, KAR9-AID*-6HA:hphNT1, ura3::pTUB1-GFP-TUB1::URA3, his3::pTEF1-osTIR::HIS3*
y3815	*MATa, DYN1-3V5-AID:KanMX6, KAR9-AID*-6HA:hphNT1, ura3::pTUB1-GFP-TUB1::URA3, his3::pTEF1-osTIR::HIS3, bfa1::TRP1*
y3816	*MATa, DYN1-3V5-AID:KanMX6, KAR9-AID*-6HA:hphNT1, ura3::pTUB1-GFP-TUB1::URA3, his3::pTEF1-osTIR::HIS3, leu2::2xYIplac128-TEM1::LEU2*
y3900	*MATa, SPC42-mScarlet-I::LEU2, yEGFP-TEM1::KanMX6, CDC15-AID*-9myc::HYG, his3::pTEF1-osTIR::HIS3*
y3901	*MATa, SPC42-mScarlet-I::LEU2, yEGFP-TEM1::KanMX6, CDC15-AID*-9myc::HYG*
y3903	*MATa, SPC42-mScarlet-I::LEU2, yEGFP-TEM1(Q79L)::KanMX6, CDC15-AID*-9myc::HYG, his3::pTEF1-osTIR::HIS3*
y3945	*MATa, yEGFP-tem1(T34A)::KanMX6, pRS316-yEGFP-TEM1, leu2::pRS305-pINO4-PfV-GS-GBP::LEU2, bfa1::TRP1*
y3948	*MATa, yEGFP-tem1(T34A)::KanMX6, pRS316-yEGFP-TEM1, bfa1::TRP1*
y3956	*MATa, yEGFP-tem1(T34A)::KanMX6, pRS316-yEGFP-TEM1, leu2::pRS305-pINO4-HOTag3-GS-GBP::LEU2*
y3958	*MATa, yEGFP-tem1(T34A)::KanMX6, pRS316-yEGFP-TEM1, leu2::pRS305-pINO4-HOTag6-GS-GBP::LEU2*
y3970	*MATa, tem1::KanMX6, pRS316-yEGFP-TEM1, leu2::pRS305-pINO4-PfV-GS-GBP::LEU2*
y3971	*MATa, tem1::KanMX6, pRS316-yEGFP-TEM1, bfa1::TRP1*
y3972	*MATa, tem1::KanMX6, pRS316-yEGFP-TEM1, leu2::pRS305-pINO4-PfV-GS-GBP::LEU2, bfa1::TRP1*
y3973	*MATa, yEGFP-TEM1::KanMX6, pRS316-yEGFP-TEM1, leu2::pRS305-pINO4-PfV-GS-GBP::LEU2*
y3974	*MATa, yEGFP-TEM1::KanMX6, pRS316-yEGFP-TEM1, bfa1::TRP1*
y3975	*MATa, yEGFP-TEM1::KanMX6, pRS316-yEGFP-TEM1, leu2::pRS305-pINO4-PfV-GS-GBP::LEU2, bfa1::TRP1*
y3976	*MATa, yEGFP-tem1(T34N)::KanMX6, pRS316-yEGFP-TEM1, leu2::pRS305-pINO4-PfV-GS-GBP::LEU2*
y3977	*MATa, yEGFP-tem1(T34N)::KanMX6, pRS316-yEGFP-TEM1, bfa1::TRP1*
y3978	*MATalpha, yEGFP-tem1(T34N)::KanMX6, pRS316-yEGFP-TEM1, leu2::pRS305-pINO4-PfV-GS-GBP::LEU2, bfa1::TRP1*
y3985	*MATa, yEGFP-tem1(T52A)::KanMX6, pRS316-yEGFP-TEM1, leu2::pRS305-pINO4-PfV-GS-GBP::LEU2*
y3986	*MATa, yEGFP-tem1(T52A)::KanMX6, pRS316-yEGFP-TEM1, bfa1::TRP1*
y3987	*MATa, yEGFP-tem1(T52A)::KanMX6, pRS316-yEGFP-TEM1, leu2::pRS305-pINO4-PfV-GS-GBP::LEU2, bfa1::TRP1*
y4095	*MATa, DYN1-3V5-AID:KanMX6, KAR9-AID*-6HA:hphNT1, his3::pTEF1-osTIR::HIS3, ura3::pTUB1-mCherry-TUB1::URA3, yEGFP-TEM1::KanMX6, leu2::pRS305-pINO4-PfV-GS-GBP::LEU2*
y4097	*MATa, DYN1-3V5-AID:KanMX6, KAR9-AID*-6HA:hphNT1, his3::pTEF1-osTIR::HIS3, ura3::pTUB1-mCherry-TUB1::URA3, yEGFP-TEM1::KanMX6*

y4100	*MATa, DYN1-3V5-AID:KanMX6, KAR9-AID*-6HA:hphNT1, his3::pTEF1-osTIR::HIS3, ura3::pTUB1-mCherry-TUB1::URA3, yEGFP-tem1(T34A)::KanMX6, leu2::pRS305-pINO4-PfV-GS-GBP::LEU2*
y4101	*MATa, DYN1-3V5-AID:KanMX6, KAR9-AID*-6HA:hphNT1, his3::pTEF1-osTIR::HIS3, ura3::pTUB1-mCherry-TUB1::URA3, yEGFP-tem1(T34A)::KanMX6, leu2::pRS305-pINO4-PfV-GS-GBP::LEU2*
y4122	*MATa, SPC42-mScarlet-I::LEU2, BFA1-yEGFP::KanMX6, TEM1(Q79L)::hphNT1, CDC15-AID*-9myc::HYG, his3::pTEF1-osTIR::HIS3*
y4123	*MATa, SPC42-mScarlet-I::LEU2, BFA1-yEGFP::KanMX6, CDC15-AID*-9myc::HYG, his3::pTEF1-osTIR::HIS3*

Table S2. Plasmids used in this study.

Plasmid	Description	Source
p998	pFA6a-link-yEGFP-SpHIS5	EUROSCARF
p1804	pRS316-eGFP-Tem1	This study
p2579	pCOLADuet-1_14xHIS-SUMO-Tem1	This study
p2717	YIplac128-Tem1 (pSP596)	S. Piatti
p2718	YIplac128-Tem1-Q79L (pSP597)	S. Piatti
p2816	pFA6a-hphN-Dbf2-HyA	This study
p2868	pFA6a-Vinnylinker-mScarlet-I-cgLEU2 (pUB1571)	E. Unal
p2888	pFA6a-hphN-Tem1Q79L	This study
p2911	pPGK1-Cas9-LEU (bRA90)	J. Haber
p2930	pFA6a-linker-yGFP(S65T)-SpHIS5	This study
p2938	pRS305-pINO4-PfV-GS-Sapphire (pLH497)	L. Holt
p3009	pFA6a-link-GBP-SpHIS5	This study
p3010	pFA6a-link-RBP-SpHIS5	This study
p3011	pRS305-pINO4-PfV-GS-GBP	This study
p3013	pRS305-pINO4-PfV-GS-RBP	This study
p3021	pCOLADuet-1-14xHIS-SUMO-Tem1Q79L	This study
p3034	pDW363_AviTag-His6-Tem1_BirA	This study
p3045	pRS305-pINO4-HOTag3-GS-GBP	This study
p3046	pRS305-pINO4-HOTag6-GS-GBP	This study